Journal of Alloys and Compounds 363 (2004) 150–174

Journal of ALLOYS AND COMPOUNDS

www.elsevier.com/locate/jallcom

Review

Microstructure, fabrication and properties of quasicrystalline Al–Cu–Fe alloys: a review

Elina Huttunen-Saarivirta*

Institute of Materials Science, Tampere University of Technology, P.O. Box 589, Tampere FIN-33101, Finland

Received 29 January 2003; received in revised form 28 March 2003; accepted 28 March 2003

Abstract

Quasicrystalline materials constitute a new materials group with certain crystalline structural characteristics, such as the generation of Bragg peaks in the X-ray data and points in the electron diffraction pattern, but translational symmetry is forbidden for crystalline materials. Thus, there exists aperiodicity in the structure of quasicrystalline materials. Besides being theoretically interesting due to their complicated atomic structure, the unique properties of quasicrystalline materials—low electrical and thermal conductivity, unusual optical properties, low surface energy and coefficient of friction, oxidation resistance, biocompatibility and high hardness, to name a few—also make them interesting for many practical purposes. Quasicrystalline phases are today encountered in over 100 alloy systems, of which the majority are aluminium based. Few of the alloying elements used to form aluminium-based quasicrystals are reasonable in price, easily available and non-toxic. However, quasicrystalline Al–Cu–Fe ternary alloys fulfill all these alloying-element criteria. In this paper, the microstructure, fabrication and properties of quasicrystalline Al–Cu–Fe alloys are reviewed from the perspective of materials engineer. The paper discusses the microstructure and metallurgy of quasicrystalline Al–Cu–Fe alloys. The preparation methods of quasicrystals in general and their application to the fabrication of Al–Cu–Fe quasicrystalline alloys are considered. The characteristics of different production methods, including both conventional methods yielding stable phases and more advanced methods introducing metastable phases, are compared in this paper. The properties of Al–Cu–Fe quasicrystals are also reviewed, aiming at a better understanding of the basic differences between crystalline and quasicrystalline materials with respect to structure and properties. Finally current and possible future applications of Al–Cu–Fe quasicrystals are discussed in the light of their properties.

Keywords: Transition metal alloys; Quasicrystals; Icosahedral symmetry

1. Introduction

In 1984 [1] a phase with a long-range orientational but an unparalleled translational order emerged in a rapidly solidified Al–Mn alloy. This discovery was at first received with considerable suspicion and criticism. However, over the last 15 years, quasicrystals have become the subject of intense theoretical study. The reason for this broad interest lies in the exceptional structure and properties of quasicrystals. Thus, on the one hand, most investigations related to quasicrystals have concentrated on these subfields of quasicrystals in general. On the other hand, much effort has been expended in finding new alloys capable of forming quasicrystalline phases. Up to now, quasicrystalline phases have been observed in over a 100 different metal alloy systems; for example, quasicrystalline alloys have been reported based on aluminium [2], copper [3], gallium [2,4], magnesium [5,6], nickel [7], tantalum [8–10], titanium [2,11,12], zinc [13–15] and zirconium [2,16–18]. As the variety of base metallic elements forming quasicrystals is wide, the spectrum of alloying elements is even wider. However, the alloying elements are often toxic, not easily available or very costly. Al–Cu–Fe alloys are an exception; these alloys are interesting due to their lack of toxicity, easy availability and the favorable costs of their alloying elements [19,20].

After two decades of quasicrystal studies, the focus of research is currently shifting closer to the reality; much interest is nowadays concentrated on finding practical production techniques and applications for these materials. The established technology of aluminium fabrication makes the Al–Cu–Fe quasicrystalline alloys more attractive than many other quasicrystalline alloys. In addition to the fabrication

* Tel.: +358-3-3115-2912; fax: +358-3-3115-2330.
E-mail address: elina.huttunen-saarivirta@tut.fi (E. Huttunen-Saarivirta).

0925-8388/$ – see front matter © 2003 Elsevier B.V. All rights reserved.
doi:10.1016/S0925-8388(03)00445-6

of Al–Cu–Fe quasicrystalline alloys, experience of their processing has been gained, for example by thermal spraying techniques. This allows the advantages of quasicrystalline Al–Cu–Fe alloys, such as their surface properties, to be emphasised, while their disadvantages, such as their room-temperature brittleness, can be compensated for by the substrate material.

Despite research work recently carried out on the microstructural details, syntheses and properties of Al–Cu–Fe alloys, no comprehensive review on them has been published. The aim of this review paper is to provide materials engineers with a shortcut to Al–Cu–Fe quasicrystals by concisely describing their microstructure, metallurgy and fabrication methods as well as their properties. The dependence of the properties of Al–Cu–Fe quasicrystals on their microstructure is discussed compared to their crystalline counterparts. This review paper also lists some current and possible future applications of quasicrystalline Al–Cu–Fe alloys.

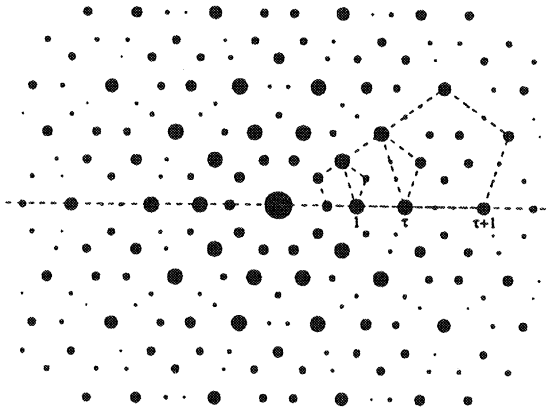

Fig. 1. The computer-generated diffraction pattern of an icosahedral quasicrystal observed along one of its five-fold symmetry directions [24]. The pentagonal symmetry is perfect around the center of the image and extends to infinity by introducing an irrational scaling factor $\tau = (1+\sqrt{5})/2$, the golden ratio. Reprinted from Ref. [24], Copyright with permission from Materials Research Society.

2. What are quasicrystals?

In solid materials composed of metallic elements, the regularity with which the atoms are arranged with respect to one another classifies structures into different categories. In non-crystalline or amorphous solids there is no systematic or periodic arrangement of atoms over large atomic distances. However, some signs of regularity in atom arrays may still be identified in an atomic distance scale [21]. In crystalline materials, in contrast, the atoms are located in a repeating, well-organised and periodic array throughout the whole structure. This periodicity embraces a set of specific rules, including, for example, the allowed rotational symmetries. Only one-, two-, three-, four- and six-fold symmetries can describe the atom stacking in crystalline materials. In practice these symmetry rules mean that the characteristics of the atom space remain unchanged after a rotation of $\frac{2\pi}{n}$, where n is one, two, three, four or six [22]. Based on this definition concerning crystalline materials, five-fold symmetry and any n-fold symmetry, where n is larger than six, are excluded [23,24].

In quasicrystalline materials, a repeating periodicity in atom arrangement exists together with rotational symmetries forbidden for crystals by definition: five-, eight-, ten- and even 12-fold symmetries have been encountered in quasicrystals [24]. With these rotational symmetries, the quasicrystals are composed of icosahedral, octagonal, decagonal and dodecagonal structural units, respectively [22,25], instead of unit cells constituting the crystals. Atoms inside the higher symmetry units are piled in an organised manner, yielding for example Bragg peaks similarly to crystalline materials. However, the inter-unit bonds orientate more freely (but not randomly) with respect to one another to form a quasicrystalline structure [25], giving rise to a translational symmetry different from that of crystalline materials. The translational symmetry indicates the amount of displacement between the individual atoms in the same direction. While crystals have planes of atoms arranged periodically, quasicrystals have their planes assembled aperiodically. Despite the aperiodicity, the planes are indeed highly ordered and their positions can be predicted by a specified irrational number $\tau = 2\cos(\pi/5) = (1+\sqrt{5})/2 = 1.618034$, called a golden ratio. The interplanar spacing in quasicrystals may, thus, vary, but this variation is somewhat controlled and repeated, as demonstrated in Fig. 1. Thus, a long-range translational order exists in quasicrystals [22].

Of quasicrystalline materials, icosahedral quasicrystals show quasiperiodicity in all three dimensions. The other classes of quasicrystals—octagonal, decagonal and dodecagonal—are quasiperiodic in two directions, in the quasiperiodic plane, and periodic in one direction, i.e. along the quasiperiodic axis [25]. Examples of some alloys exhibiting quasicrystalline structures of icosahedral, octagonal, decagonal and dodecagonal symmetry are collected in Table 1.

3. Structure of Al–Cu–Fe quasicrystals

3.1. Current theoretical approaches

Al–Cu–Fe quasicrystals show a five-fold symmetry and are, thus, icosahedrally structured. An icosahedron is a polyhedron having 20 equilateral triangles, as shown in Fig. 2. Today, two models are generally used to describe icosahedral and other quasicrystalline structures; the Penrose model and the quasi-unit cell theory. Previously the glass model, random-tiling model and twinned crystal model were proposed to explain the real quasicrystalline structures, but nowadays none of them receives very much support.

Table 1
Examples of some alloys exhibiting quasicrystalline structures of icosahedral, octagonal, decagonal and dodecagonal symmetry

Structure of quasicrystal	Alloys
Icosahedral	Al–Cu–Fe, Al–Mn, Al–Mn–Si, Al–Mn–Cu, Al–Mn–Zn, Al–Cu–Ru, Al–Cu–Os, Al–Cr, Al–V–Si, Al–Pd–Ru, Al–Pd–Mn, Al–Pd–Re, Al–Pd–Mg, Al–Li–Cu, Al–Mg–Zn, Al–Rh–Si, Ti–Fe–Si, Ti–Zr–Ni, Mg–Li–Al, Mg–Zn–Y, Mg–Zn–Ho, Cd–Mg–Tb
Octagonal	Ni–Cr–Si, Ni–V–Si, Mn–Si
Decagonal	Al–Mn, Al–Fe, Al–Pd, Al–Pd–Fe, Al–Pd–Ru, Al–Pd–Os, Al–Os, Al–Co–Ni, Al–Cu–Co, Al–Cu–Fe–Co, Al–Cu–Co–Si, Al–Co–Fe–Cr–O, Al–Cr–Si, Al–Ni–Fe, Al–Ni–Rh, Al–Cu–Rh, Zn–Mg–Y, Zn–Mg–Sm, Zn–Mg–Ho
Dodecagonal	Ni–Cr, Ni–V, Ni–V–Si, Ta–Te, Co–Cu, Al–Co–Fe–Cr

The Penrose model suggests that quasicrystals are composed of two or more unit cells, tilings, that fit together according to specific matching rules. Two most common Penrose tilings are thin and fat rhombuses, with equal edge lengths as well as angles of 36° and 144°, and 72° and 108°, respectively. These Penrose tilings have pentagonal orientational symmetry [26]. Generally, certain empirical rules known as matching rules can be employed to fill the plane. Besides matching rules, geometrical methods can be used to treat the existing tilings with different mathematical algorithms [27–33] to fill the space efficiently.

When Penrose tilings are put together to fill the plane, they give rise to a five-fold pattern in a four-dimensional reciprocal space. This is due to the fact that the projection of periodic sequence in two dimensions can yield an aperiodic sequence in one dimension [22]. Two-dimensional aperiodic Penrose tilings are, thus, presented in a four-dimensional space by five basic vectors, four of which are independent. When the whole space is covered by Penrose tilings instead of a plane, a three-dimensional icosahedral lattice may be embedded in a six-dimensional space. Sometimes this six-dimensional space can be thought to be constituted of two three-dimensional orthogonal subspaces, one of which is real and called a physical space $E_{||}$. The other subspace, consisting of the remaining three dimensions, is called a perpendicular space $E_{\perp}$ [22,34]. However, the structure giving rise to a six-dimensional reciprocal space cannot be treated by the conventional indexing method, which is based on a three-dimensional reciprocal lattice. Thus, the Miller indices do not suffice for the structures of icosahedral symmetry. A new method for indexing the icosahedral structure in a six-dimensional space has been proposed by Bancel et al. [35]. This new means of indexing makes use of six independent vectors, which point to the vertices of an icosahedron. They are generated by cyclic permutations of $(q_x, q_y, q_z) = (\pm 1, \pm \tau, 0)$, yielding vectors $q_1 = (1, \tau, 0)$, $q_2 = (1, -\tau, 0)$, $q_3 = (0, 1, \tau)$, $q_4 = (0, 1, -\tau)$, $q_5 = (\tau, 0, 1)$ and $q_6 = (-\tau, 0, 1)$, where τ is the golden mean, $(1+\sqrt{5})/2$. This indexing can be employed when studying the structure of icosahedral phases by using either X-ray or electron diffraction patterns.

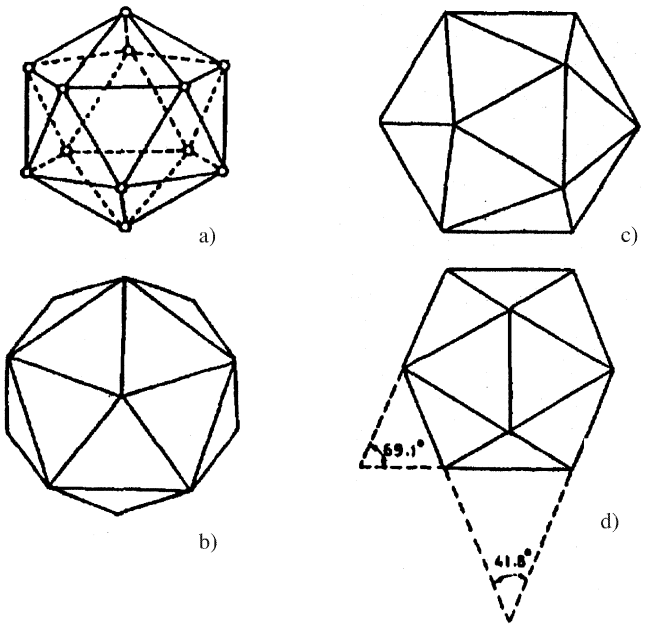

Fig. 2. The shape of an icosahedron from different projections according to Ref. [43]. (a) A general view, (b) along the five-fold axis, (c) along the three-fold axis, (d) along the two-fold axis. Reprinted from Ref. [43], Copyright with permission from Elsevier.

The Penrose model was among the first to explain the quasiperiodic structures. However, it has difficulties explaining the atom-scale growth processes involved in the build-up of a quasicrystalline structure. In contrast, discoveries concerning the formation of quasicrystalline structure are explained well by the quasi-unit cell theory, which is quite a recent approach to treat quasicrystalline structures. In quasi-unit cell theory, quasicrystals are described in terms of a single, closely-packed repeating cluster of low energy [36]. The repeating cluster is equivalent to the unit cell in periodic crystals. The key difference from the Penrose model, however, is that the atomic arrangement in the case of quasicrystals is constrained to allow atom sharing

among neighboring clusters [37–40]. This atomic sharing works for only special atom arrangements and causes clusters to orientate according to certain rules or randomly with respect to another. This random orientation violates the Penrose model, since the symmetry conservation is not fulfilled. Besides the atom sharing, individual clusters can overlap to adjust to required geometries. It is also proposed that these intercluster bondings are weaker than those holding the individual clusters together [40]; the advantages of the quasi-unit cell theory include its ability to separate the inter- and intra-cluster bonds, which are in the key role for the formation of the quasicrystalline structure.

3.2. Real structures of quasicrystalline Al–Cu–Fe alloys

Regardless of existing theoretical models to study the quasicrystalline structure, there are no unambiguous solutions as to why and how these aperiodic quasicrystalline structures form in reality. According to Dmitrienko et al. [41], quasicrystals consist of large atomic clusters in a melt state, while the degree of clustering is decreased in the quasicrystal solidification process. During nucleation, the local atomic order is supposed to be similar to that found in crystalline materials, whereas the quasiperiodic long-range structure develops during the growth process according to statistical and energetical criteria [41]. Thus, not surprisingly, the driving force for quasicrystal formation is suggested to be the minimisation of the system free energy [42,43]. According to Chattopadhyay et al. [43], quasicrystals grow in a faceted manner. The faceted quasicrystalline interface grows stepwise, the growth step being much larger than for crystalline materials. Furthermore, the morphology of quasicrystals often reflects the inherent non-crystallographic symmetry.

Icosahedral quasicrystalline structures are known to be composed of a quasiperiodic arrangement of icosahedral atomic clusters [44,45]. The icosahedral packing of atoms may take place in two ways. The atom stacking can, accordingly, be categorised into clusters of either Mackay icosahedron (MI) type or triacontahedron (TC) type. The MI-type icosahedral clusters contain aluminium and transition metal atoms, and there are glue atoms between individual clusters. It is generally admitted that Al–Cu–Fe quasicrystals represent a face-centered icosahedral structure of Mackay icosahedral type [46,47]. In contrast, the TC-type quasicrystals contain simple sp-metal elements instead of transition metal elements. In the TC-type the unit of packing is a triacontahedral atom cluster and the packing does not require any glue atoms [47]. The classification of icosahedral structures into MI- or TC-types is related to differences in structure stability; specific intermetallic compounds arise preferentially in the characteristic ranges of the valence concentration e/a, known as the Hume-Rothery rule [48–51]. The icosahedral structure of Mackay type (MI) shows typical electron-to-atom ratio values of 1.6–1.8, while triacontahedron type (TC) icosahedral structures are formed by conforming to the electron-to-atom ratio of 2.1–2.25 [44,47,51]. The narrow range of the valence concentration for icosahedral quasicrystals implies that the stable quasicrystals are essentially formed by the Hume-Rothery electron mechanism [47]. This also allows the determination of alloy compositions capable of quasicrystal formation [50]. However, although the Hume-Rothery rule is shown to work for Al–Cu–Fe icosahedral quasicrystals, this is not the case for all quasicrystalline structures. For example, some stable decagonal quasicrystals form over a wide compositional range, throwing doubt on the exact determination of the position of quasicrystalline phases in phase diagrams [51]. Still, the Hume-Rothery rule offers an interesting approach to study existing quasicrystalline structures and to find new quasicrystalline phases.

Inside the atomic clusters, the location of individual atoms is of interest. Sadoc [52] has compared how the different atoms cluster in various stable aluminium-based quasicrystalline alloys containing copper or iron. The short-range order in Al–Cu–Fe quasicrystals is different around Cu and Fe atoms. The environment of Cu atoms in Al–Cu–Fe looks like that found around V atoms, but differs from that around Cu atoms, in Al–Cu–V. The neighborhood of an Fe atom, instead, resembles that obtained around Mn in Al–Mn and Al–Mn–Si quasicrystals, or even around Fe and Cr in Al–Fe–Cr or Cu in Al–Cu–V. This could only result from the existence of at least two different atomic sites. The fact that Cu and Fe atoms do not occupy the same sites is best explained by their different valence electron counts [52]. In contrast to Sadoc, Müller et al. [53] have compared the atomic decoration and short-range order of the icosahedral Al–Cu–Fe alloys to those of its crystalline counterparts. According to Müller et al., the short-range order in the icosahedral phase has some similarity with that occurring around iron sites with ten nearest neighbors being aluminium atoms in the crystalline structure of $Al_{13}Fe_4$. Brand et al. [54,55], in turn, have established that in icosahedral $Al_{62}Cu_{25.5}Fe_{12.5}$ alloy, the Cu atoms are surrounded by 12 Al atoms on an icosahedron and 20 Al, Cu and Fe atoms on a dodecahedron. This structure forms a cluster of 33 atoms. Iron and copper have different places and effects on the structure, which is reflected in different jumping times during diffusion and other atom movements; iron atoms jump two orders of magnitude slower than copper. Thus, there is generally consensus on the different positions or Cu and Fe atoms inside atomic clusters.

Not only the structural arrangement on an atomic level, but also the electronic structure of quasicrystals is quite unusual. For quasicrystalline materials, in general, a pseudogap, i.e. an extended depression, is assumed in the density of electron states [47], in contrast to crystalline materials. For Al–Cu–Fe quasicrystals, this pseudogap is observed to be extremely deep, which is suggested to be due to its characteristic value for the Hume-Rothery e/a ratio [44,56]. Thus, the local order characteristics of quasiperiodicity have a pronounced effect on electronic confinement [57,58].

4. Synthesis of quasicrystals

The structural characteristics of quasicrystals influence their synthesis and processing methods. Earlier it was mentioned that the Hume-Rothery rule is applicable to certain stable quasicrystals. However, not every quasicrystal is stable; thermodynamically metastable quasicrystalline phases also exist. Al–Cu–Fe happens to be stable, but can be obtained in a metastable form by suitable synthesising methods.

The formation of stable quasicrystals may normally be predicted by equilibrium phase diagrams. They can, thus, be prepared by conventional equilibrium processes utilising melting and solidification procedures [24,51]. In contrast, the metastable phase is in a non-equilibrium state, which, despite the fact that it may persist for a very long time [21], cannot be treated by thermodynamical equilibrium rules. Therefore, metastable quasicrystals can only be synthesised by employing more advanced methods.

Altogether, the preparation methods known to produce quasicrystalline materials include the solidification of molten alloys, rapid quenching techniques such as melt spinning and gas atomisation, mechanical alloying, electrodeposition, physical vapor deposition, gas evaporation, laser- or electron-beam superficial fusion and electron irradiation. In addition to these methods to directly produce quasicrystalline materials, the low-temperature annealing of amorphous phases or the high-temperature heat treatment of crystalline intermetallic phases or even stacks of pure-element layers can be used to yield quasicrystalline phases [23,59–68]. The characteristics of the four most common fabrication methods of Al–Cu–Fe quasicrystals, i.e. melting accompanied by solidification obeying thermodynamic principles, rapid solidification in the form of melt spinning and gas atomisation as well as mechanical alloying, are compared in Table 2.

The most common method for preparing stable quasicrystals in the laboratory is to melt the pure constituents and cast the melt into ingots. Tube-like shapes have also been fabricated [69]. Generally, the casting process is carried out under vacuum or inert atmosphere, since many alloys, including Al–Cu–Fe alloys, capable of forming quasicrystalline phases are easily oxidised. For most known alloys and compositions, quasicrystalline phases form by peritectic solidification of high temperature crystalline phases reacting with the residual liquid. This process is necessarily slow, and most usually some crystalline constituent is retained in the sample at room temperature together with the quasicrystal. Also, since crystals and quasicrystals exhibit significant composition and atomic volume differences, pores usually form at this stage with sizes distributed up to micrometer range [70,71]. To overcome the difficulties linked with the co-existence of crystalline and quasicrystalline phases and the uncontrolled development of pores, a powder mixture of the desired composition may be sintered above the peritectic reaction temperature. Sintering is a simple technique to prepare bulk specimens of controlled microstructure, including single-phase icosahedral Al–Cu–Fe samples of stoichiometric composition. Desired mixtures of quasicrystals and crystals may also be produced by adjusting the composition of the initial powder or using a mixture of various powders [71]. Besides the preparation of polycrystals, the growth of quasicrystalline single crystal samples from melt is also possible for stable quasicrystal-forming systems [13,51,72,73], but requires a careful process control.

All quasicrystalline phases are not thermodynamically stable, as previously discussed. Therefore, purely quasicrystalline material cannot always be fabricated by conventional casting and heat treatment procedures. Instead, the rapid solidification techniques of the melt can be applied [74]. Rapid solidification may introduce substantial extension into the solid solubility of alloying elements into the base metal and yield new non-equilibrium structures, thus allowing the production of metastable quasicrystals [75]. Rapid solidification techniques aim to retain the high-temperature microstructure at lower temperatures, generally at room temperature, by solidifying the melt so rapidly that the microstructural changes have no time to take place. Melt spinning is the most commonly used rapid solidification technique at present and, for example, the only method for the preparation of some metastable quasicrystalline alloys such as Al–Mg–Cu [76–78]. It was also the first method utilised to produce quasicrystalline materials [51].

Melt spinning is a rapid quenching technique for molten alloys, where the liquid metal is ejected from a nozzle and impinges on the outer surface of a rotating copper roller. Typical quenching rates reached by the melt-spinning technique are $\sim 10^4$–10^7 °C/s [51]. Rapid solidification of the melt is aimed at producing a continuous ribbon [79], although the quasicrystals thus prepared are typically in the form of brittle ribbons or flakes [69,80]. This somewhat makes their further preparation in bulk samples quite difficult [69]. However, the microstructure and properties of melt-spun ribbons are very sensitive to processing parameters [79,80], introducing the means to pursue the formation of quasicrystals of desired structure. The quenching rate of the melt-spinning process may be increased by increasing the wheel speed, by changing the ambient gas, by decreasing the temperature of the melt or by increasing the ejection pressure [79]. A higher quenching rate produces thinner ribbons and a finer quasicrystalline microstructure [80].

Gas atomisation is another available rapid solidification technique. The quenching rates attainable by gas atomisation are somewhat higher that those reachable by melt spinning. Gas atomisation can be described simply as the break-up of a molten metal into fine droplets, typically smaller than 150 μm. Increasing the superheat of the melt introduces a finer particle size [81]. Many of the available commercial quasicrystalline powders are produced by gas atomisation because of its ability to generate powders of circular form and good flowing properties. Due to the sphericity of the produced powder particles, gas atomised

Table 2
Comparison of the common fabrication process characteristics of quasicrystals

	Melting and solidification	Melt spinning	Gas atomisation	Mechanical alloying
Suitable for quasicrystals of thermodynamical stability	Stable	Metastable	Metastable	Metastable
Phase structure of quasicrystalline products	Single-phase structure generally achieved by successive heat treatment	Single-phase structure achievable both directly and by successive heat treatment	Single-phase structure achievable both directly and by successive heat treatment	Single-phase structure achievable both directly and by successive heat treatment
The shape of quasicrystalline products	Desired	Thin ribbon	Powder with a grain size smaller than 150 μm	A fine powder with a layered structure
Quality of produced quasicrystals	High, sharp X-ray diffraction peaks, pores may exist in the structure if crystalline phases coexist	Broadening of X-ray peaks may occur; phasons	Generally high, sharp X-ray diffraction peaks	Broadening of X-ray peaks may occur, phasons; the ordering of the face-centered structure may not be complete
Contamination resources	Air	Air	Air	Air, grinding media, grinding vessel
Further processing possibilities	Heat treatment	Compaction, grinding and compaction, (heat treatment; quasicrystalline phases may decompose during annealing)	Thermal spraying, compaction, sintering, mechanical alloying, (heat treatment)	Compaction, thermal spraying, (heat treatment)

powders can be used in thermal spraying processes and other powder metallurgical processes such as compaction and sintering as well as mechanical alloying.

Besides the rapid solidification methods, mechanical alloying is another method to extend the solubility limits of the alloying elements into the base material [82,83]. Accordingly, metastable quasicrystalline materials can be directly prepared by mechanical alloying of elemental powders [83–86]. In addition, mechanical alloying allows alloying of powder in the solid state, avoiding melting and solidification. Mechanical alloying begins by charging the elemental powder mixture (quantities according to the composition of the expected product), grinding media (generally steel balls) and the process-controlling agent into the grinding vessel. The mill then starts to vibrate causing the steel balls to collide with each other, the powders being located between the colliding balls. Ball milling produces powder of the expected composition with a layered microstructure. The latter forms as a result of the millings becoming repetitively fractured and welded together [75,83]. For the formation of quasicrystalline powders, interdiffusion is necessary in addition to sequential fracturing and welding [87]. However, although the powder mixtures of quasicrystal-forming elements are mechanically alloyed, no quasicrystalline phases necessarily form, as demonstrated by Ji et al. [82]. The milling conditions strongly influence phase selection. With low milling intensity, an amorphous phase instead of a quasicrystalline phase forms. High-intensity milling conditions or milling for too long results in the formation of a crystalline powder. In between, suitable conditions for quasicrystal formation exist [86–88]. In some cases, post-annealing treatment of the milled powder has to be performed to obtain the quasicrystalline structure [74].

Industrial methods to make quasicrystalline products generally use existing quasicrystalline powders. Commercial quasicrystalline powders prepared by gas atomisation are already available. Thick coatings can be obtained by plasma spraying the powder onto the substrate material.

This plasma-sprayed coating is substantially a composite material, comprising not only of the deposited quasicrystals but also pores, cracks and oxides [70,89]. Another method to use quasicrystals on an industrial scale is the manufacture of bulk composites. A precipitation-hardened steel, an Al-based alloy, which can be formed by rapid solidification and powder processing, and metal–matrix composites incorporating quasicrystalline powders into an aluminium-based alloy have been proposed [19,70,90,91]. New industrial processes for preparing quasicrystalline materials are also currently being sought.

5. The Al–Cu–Fe system and quasicrystalline phase formation during synthesis

Intermetallic ternary alloy phase diagrams are rarely perfect, and are often not available for all ternary systems [73]. Fortunately, the Al–Cu–Fe ternary system has received much attention lately. Some basic principles of the system thermodynamics are therefore known. Section 5.1 focuses on the Al–Cu–Fe equilibrium system and quasicrystalline phase formation under conditions yielding stable phases. As discussed in Section 4, however, not every fabrication process maintains the thermodynamic equilibrium conditions. Section 5.2 concentrates on these processes introducing metastable quasicrystalline phases into the Al–Cu–Fe system.

5.1. The Al–Cu–Fe system in equilibrium

Bradley and Goldschmidt [92] were the first to reveal the compositional formation area and the phase relations of the icosahedral quasicrystalline phase in the ternary Al–Cu–Fe system; the phase was then called an unknown ψ-phase. Its ideal formula was proposed to be Al_6Cu_2Fe and its average composition in the single-phase region $Al_{65}Cu_{22.5}Fe_{12.5}$. Bradley and Goldschmidt reported the build-up of an (unknown) icosahedral phase resulting from a peritectic reaction between the β-$AlFe_3$ phase and the remaining liquid. The aluminium-rich portion of the Al–Cu–Fe ternary phase diagram outlined by them is shown in Fig. 3. The most important binary and ternary phases in the Al–Cu–Fe system are summarised in Table 3.

Another Al–Cu–Fe phase diagram at room temperature is sketched by Faudot et al. [93]. A single-phase quasicrystalline structure is obtainable with the compositions $Al_{61.75–64}Cu_{24–25.5}Fe_{12–12.75}$, as indicated in Fig. 4. However, the icosahedral phase is attainable within the compositional range of 20–28 at.% Cu and 10–14 at.% Fe up to a

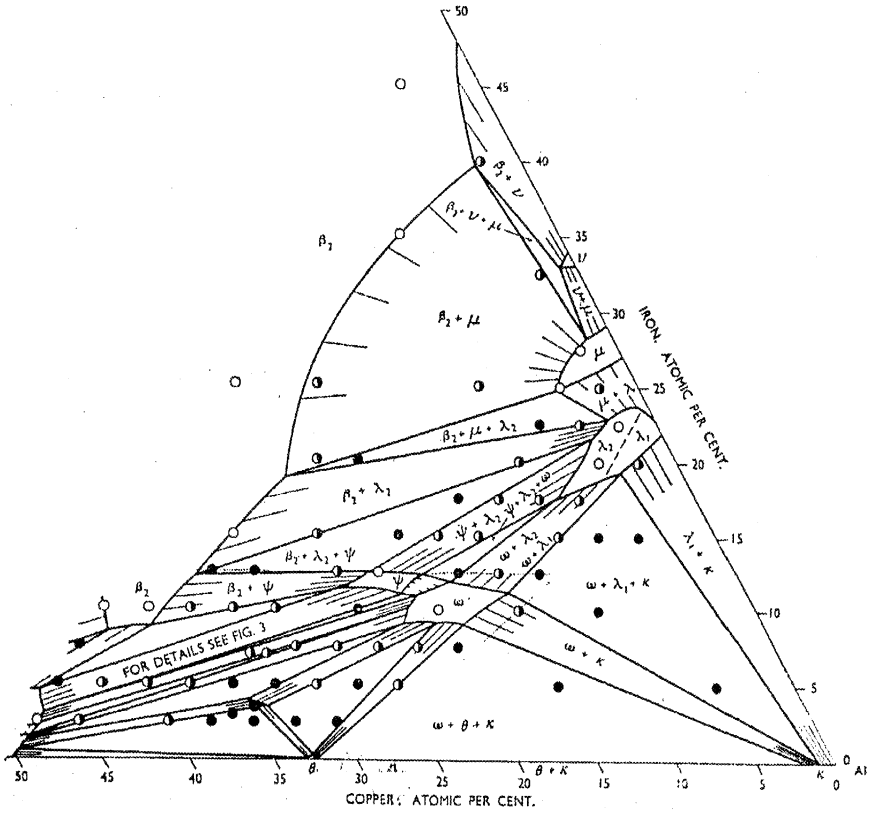

Fig. 3. The aluminium-rich portion of aluminium–copper–iron constitutional diagram according to Ref. [92]. White circles show the single-phase areas, black and white circles indicate the two-phase areas and black circles express the simultaneous presence of three phases. Reprinted from Ref. [92], Copyright with permission from Maney Publishing.

Table 3
The most important binary and ternary phases and their structures in the Al–Cu–Fe system

Phase	Ideal formula	Structure, composition	Reference
η	AlCu	Orthorhombic, related to δ-type Ni_2Al_3	[90,91,93,94]
τ	AlCu (Fe)		[96]
θ	Al_2Cu	Tetragonal	[93,94,106]
λ	Al_7Fe_2	Orthorhombic	[90]
λ_1, λ_2	Al_3Fe	Different amounts of Cu dissolved	[93,94]
λ	$Al_{13}Fe_4$	Monoclinic	[96,99,101]
μ	Al_5Fe_2	Monoclinic	[90,99]
β_1	$AlFe_3$	Body-centered cubic with superlattice	[90]
β	$Al_5(Cu,Fe)_5$, AlFe(Cu)	Cubic (CsCl type)	[96,99]
ϕ	$Al_{10}Cu_{10}Fe$	Related to δ-type Ni_2Al_3	[90,99]
χ	$Al_{18}Cu_{10}Fe$	Related to ϕ	[90,91,93,94,99]
ψ	Al_6Cu_2Fe	Icosahedral	[90]
ω	Al_7Cu_2Fe	Tetragonal	[90,91,93,94,101]

temperature of 860 °C, as shown in Fig. 5. This temperature indicates the onset of a peritectic reaction, through which the icosahedral phase forms from the melt under equilibrium conditions. Here, the peritectic reaction responsible for the icosahedral phase formation is suggested to occur between λ_2-Al_3Fe phase, β-AlFe(Cu) and the liquid; Gui et al. [94] later agreed with this suggestion. For the Al–Cu–Fe alloy of composition $Al_{62}Cu_{25.5}Fe_{12.5}$, the X-ray diffraction lines of the quasicrystalline phase are narrow independently of whether the annealing temperature is 800 or 600 °C. Thus, between these temperatures there exists a single-phase region where the quasicrystalline phase is structurally perfect and remains stable.

The results concerning the stability area and the formation of the Al–Cu–Fe quasicrystalline phase at higher temperatures somewhat deviate from each other. Above, the icosahedral phase was stated to form within the compositional range 20–28 at.% Cu and 10–14 at.% Fe up to a temperature of 860 °C [93]. The pseudo-binary phase diagram constructed by Yokoyama et al. [95,96] for the Al–Cu–Fe system at higher temperatures is shown in Fig. 6. Again, the formation of the quasicrystalline phase in the Al–Cu–Fe alloy system occurs by the peritectic reaction. However, the reaction takes place only between the λ_2-Al_3Fe phase and the liquid. This reaction occurs at ∼820 °C (at 1090 K in Fig. 11) [95,96], which is 40 °C lower than that proposed by Faudot et al. [93]. Below the peritectic reaction temperature, the icosahedral phase stability area extends over the whole vertical section $Al_{65}Cu_{35-x}Fe_x$, where x is from 0 to 20 at.%. Although no other studies have reported such a wide compositional stability area for the icosahedral phase in the Al–Cu–Fe system, the single icosahedral phase area exists over a very limited composition range, namely at $Al_{65}Cu_{20}Fe_{15}$.

Tsai et al. [60] were the first to report the thermodynamical stability of the icosahedral phase in a conventionally melted and solidified $Al_{65}Cu_{20}Fe_{15}$ alloy. In contrast to the demonstrations of Tsai et al. and the phase diagrams presented in the previous section, Van Buuren et al. [97]

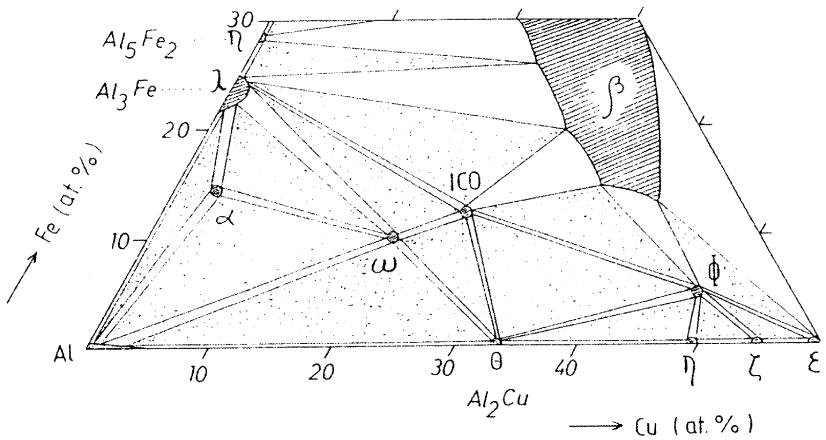

Fig. 4. Portion of the Al–Cu–Fe constitutional diagram at room temperature according to Ref. [93]. Dashed area: single-phase ranges; white area: two-phase ranges; dotted area: three-phase ranges. Reprinted from Ref. [93], Copyright with permission from Elsevier.

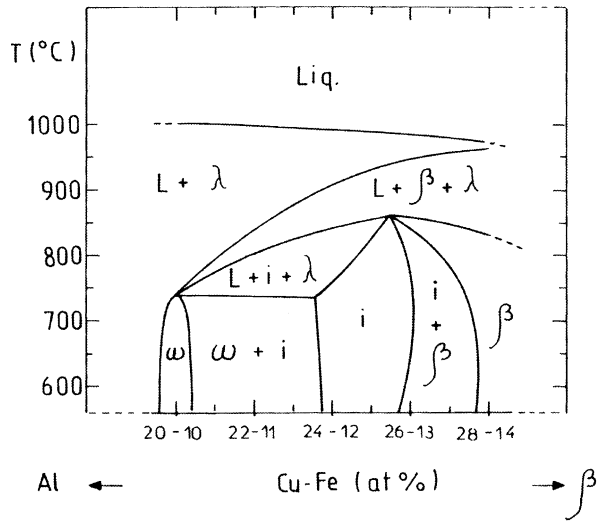

Fig. 5. Pseudo-binary Al–Cu–Fe phase diagram in the range of compositions of the quasicrystalline (i) phase between ω ($Al_{70}Cu_{20}Fe_{10}$) and $Al_{58}Cu_{28}Fe_{14}$ according to Ref. [93]. Reprinted from Ref. [93], Copyright with permission from Elsevier.

observed that the quasicrystalline phase in $Al_{65}Cu_{20}Fe_{15}$ alloy transforms partly into the λ-$Al_{13}Fe_4$ phase in a thermally activated process with an activation energy of the order of 300 kJ/mol [97].

An alloy of composition $Al_{62}Cu_{25.5}Fe_{12.5}$ has been found by Lee et al. [98] to be composed of an icosahedral phase in addition to the β-AlFe(Cu) and τ-AlCu(Fe) phases as well as small amounts of the λ-$Al_{13}Fe_4$ phase. It is worth noting that no other studies report the formation of the τ-phase under equilibrium conditions. In the alloy $Al_{62}Cu_{25.5}Fe_{12.5}$, the icosahedral phase formation is demonstrated to take place by a peritectic reaction between the primary β-phase and the

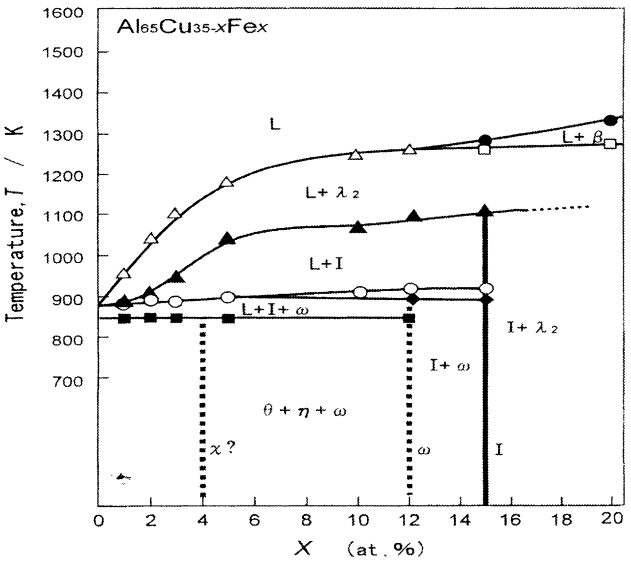

Fig. 6. Pseudo-binary phase diagram along an $Al_{65}Cu_{35-x}Fe_x$ ($x = 0$–20 at.%) composition line according to Ref. [95]. Reprinted from Ref. [95], Copyright with permission from Elsevier.

liquid melt. However, only after heat treatment at 750 °C for 3 h, is a single-phase icosahedral structure obtained, while annealing at 850 °C for 3 h yields a structure where the icosahedral phase coexists with the β- and λ-phases [98]. Thus, according to Lee et al., no single-phase icosahedral structure is obtainable in $Al_{62}Cu_{25.5}Fe_{12.5}$ without further heat treatments.

An important reminder of the character of the phase diagrams is made by Gui et al. [94]. They emphasise that the composition of each of the phases is different in different alloys. For example, the equilibrium composition of the icosahedral phase after annealing at 800 °C is $Al_{60.7}Cu_{25.5}Fe_{13.8}$ in the $Al_{65}Cu_{20}Fe_{15}$ alloy and $Al_{58.4}Cu_{28.6}Fe_{13}$ in the $Al_{62.5}Cu_{25}Fe_{12.5}$ alloy. This is because the icosahedral phase is attainable within a composition range of a few atomic percents. In the $Al_{65}Cu_{20}Fe_{15}$ alloy the icosahedral phase is in equilibrium with the Cu-poor λ-$Al_{13}Fe_4$ phase, while in the $Al_{62.5}Cu_{25}Fe_{12.5}$ alloy it is in equilibrium with the Cu-containing β-phase. Thus, the quasicrystalline phase in $Al_{65}Cu_{20}Fe_{15}$ alloy contains less Cu compared to that in $Al_{62.5}Cu_{25}Fe_{12.5}$ alloy. This observation indicates that the composition of the icosahedral phase in Al–Cu–Fe alloys depends not only on the cooling condition and the equilibrium temperature but also on the coexisting phases that are in equilibrium with the icosahedral structure [94].

5.2. Processes yielding metastable quasicrystalline phases in Al–Cu–Fe system

In the present section, processes introducing metastable quasicrystalline phases in Al–Cu–Fe alloys, i.e. rapid solidification methods and mechanical alloying, are discussed in terms of process variables, alloy compositions and formed microstructure.

5.2.1. Moderate rate or rapid solidification—do they yield differences in specimen microstructure?

The icosahedral phase is stable at high temperatures over a compositional range of several atomic percents. Fig. 7 shows the stability area of the melt-spun quasicrystalline phase in the Al–Cu–Fe system at 650 °C and Fig. 8 that at 750 °C. In turn, the isothermic section of the ternary Al–Cu–Fe system at 850 °C is represented in Fig. 9. In contrast to studies carried out at 650 and 750 °C, the icosahedral phase cannot be obtained as a single-phase region at 850 °C. At this temperature the cubic β-AlFe(Cu) phase always coexists with the icosahedral phase. However, nucleation of the quasicrystalline phase is obtained in a wide compositional range as proposed by Waseda et al. [99,100], the amount of the icosahedral phase being strongly dependent on the iron concentration in the alloy [101]. Thus, from the materials engineer's point of view, maintenance of the microstructure typical for a temperature of 750 °C during the rapid solidification process would be most beneficial, since the stability area of the single icosahedral phase is there the widest among the studied temperatures.

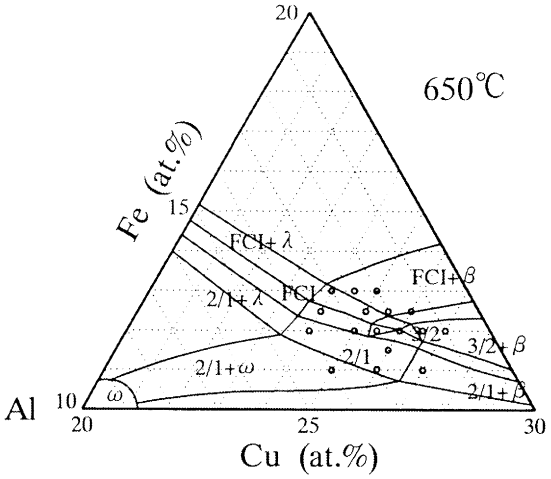

Fig. 7. Approximate isothermic section of the ternary Al–Cu–Fe phase diagram near the icosahedral phase forming region at 650 °C according to Ref. [99]. Reprinted from Ref. [99], Copyright with permission from Japan Institute of Metals.

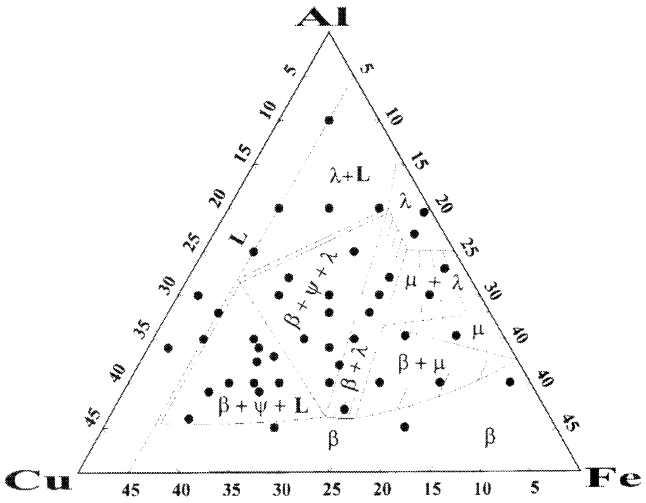

Fig. 9. The isothermic section of the ternary Al–Cu–Fe system at 850 °C according to Ref. [101]. Reprinted from Ref. [101], Copyright with permission from Elsevier.

Rosas and Perez [102] have compared the structural and chemical characteristics of phases which exist in moderately and rapidly quenched Al–Cu–Fe alloys. They have demonstrated that the icosahedral phase forms at ∼884 °C in the composition ranges 54–75 at.% Al, 21–31 at.% Cu and 7.5–16.5 at.% Fe by the mechanism suggested by Bradley and Goldschmidt [92]. Both moderate and rapid solidification gave rise to the same type of phase transformations in specimens when heat treated under similar temperature conditions [102]. When annealed in the temperature range 700–850 °C, three different dissolution types of the icosahedral phase may occur. In the case of alloy $Al_{60}Cu_{25}Fe_{15}$, the icosahedral phase is directly transformed to the monoclinic structure λ-$Al_{13}Fe_4$ at 700 °C [103]. This is analogous to the influence of thermal activation on the icosahedral phase in the $Al_{65}Cu_{20}Fe_{15}$ alloy reported by Van Buuren et al. [97]. For the compositional values of $Al_{58}Cu_{28}Fe_{14}$, the ψ-Al_6Cu_2Fe icosahedral phase is completely transformed into the β-AlFe(Cu) cubic phase at 700 °C. Depending on the composition of the Al–Cu–Fe alloys and on the annealing treatment after quenching, this crystalline β-AlFe(Cu) displays variations in the lattice parameter, which is due to variation in the amount of Cu and Fe in the β-solid solution. Another transformation of the icosahedral phase is observed for the composition $Al_{68}Cu_{27}Fe_5$, where a tetragonal ω-Al_7Cu_2Fe structure is finally obtained. At ∼700 °C, an alloy with the composition of $Al_{64}Cu_{24}Fe_{12}$ produces a single icosahedral phase [103]. This suits well with the observations of Faudot et al. [93].

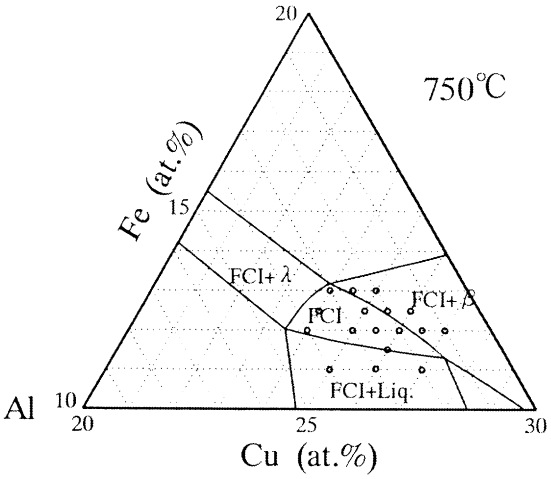

Fig. 8. Approximate isothermic section of the ternary Al–Cu–Fe phase diagram near the icosahedral phase forming region at 750 °C according to Ref. [99]. Reprinted from Ref. [99], Copyright with permission from Japan Institute of Metals.

If no post-annealing treatment is employed for samples solidified at moderate rate or rapidly, however, some differences in their microstructures are evident. Holland-Moritz et al. [104] have explored quasicrystal formation in moderately and rapidly quenched Al–Cu–Fe alloys with the compositions $Al_{62}Cu_{25.5}Fe_{12.5}$ and $Al_{60}Cu_{34}Fe_6$. When the moderate cooling rate (10^1-10^2 °C/s) is used, $Al_{62}Cu_{25.5}Fe_{12.5}$ alloy primarily produces λ-$Al_{13}Fe_4$ and β-AlFe(Cu) phases. Finally the icosahedral quasicrystalline phase of composition $Al_{65.7}Cu_{19.8}Fe_{14.5}$ is formed by the peritectic reaction. For $Al_{60}Cu_{34}Fe_6$, the morphology and phase distribution are similar to those of $Al_{62}Cu_{25.5}Fe_{12.5}$ with the exception that the fraction of the Cu-rich phases is higher [104]. When higher cooling rates are employed for $Al_{62}Cu_{25.5}Fe_{12.5}$, the λ-$Al_{13}Fe_4$ phase primarily forms, followed by the build-up of the icosahedral phase exhibiting the composition $Al_{61.4}Cu_{25.5}Fe_{13.1}$. Finally, the τ-phase is formed [104,105]. Thus, when higher cooling rates are employed or when undercooling is high enough, a change in the phase selection occurs and no λ-phase can be detected

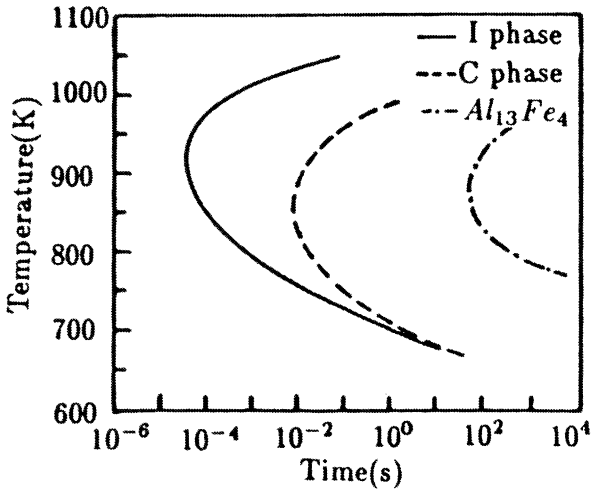

Fig. 10. Calculated TTT curves of the λ-$Al_{13}Fe_4$ phase, cubic β-phase (C) and icosahedral (I) phases as a function of temperature in the Al–Cu–Fe alloy according to Ref. [106]. Reprinted from Ref. [106], Copyright with permission from Elsevier.

in the final structure. In $Al_{62}Cu_{25.5}Fe_{12.5}$, cooling rates of 10^6 °C/s and higher directly produce the icosahedral phase. In $Al_{60}Cu_{34}Fe_6$, a cooling rate of 10^2 °C/s primarily yields the icosahedral phase [104].

As discussed above, phase selection during solidification of Al–Cu–Fe alloys strongly depends on the processing conditions. The phase selection changes in a similar way with increasing cooling rate and with increasing undercooling; both high cooling rate and pronounced undercooling promote the formation of the icosahedral Al–Cu–Fe phase [104]. Fig. 10 [106] demonstrates the influence of cooling rate on the formation of different phases in Al–Cu–Fe alloy melts.

Despite the strong influence of the processing conditions on phase selection in Al–Cu–Fe alloys, other parameters such as composition naturally influence the eventual microstructure. For moderately and rapidly quenched Al–Cu–Fe alloys exhibiting the compositions $Al_{65}Cu_{20}Fe_{15}$ and $Al_{62.5}Cu_{25.5}Fe_{12}$, the phase selection typical for alloys with higher alloying element concentrations (discussed above) is not valid any more. The moderate cooling rate causes the formation of λ-$Al_{13}Fe_4$, β-AlFe(Cu), icosahedral quasicrystalline and τ-AlCu(Fe) phases in the solidified $Al_{65}Cu_{20}Fe_{15}$ alloy. During subsequent annealing treatment at 750 °C for 3 h, a significant decrease in the amount of icosahedral phase occurs. For alloy $Al_{62.5}Cu_{25.5}Fe_{12}$, the presence of β-AlFe(Cu), τ-AlCu(Fe) and icosahedral phases is detected after moderate quenching. When heat treated at 750 °C for 3 h, a nearly homogeneous icosahedral single-phase structure can be obtained. Due to the moderate cooling rate, the icosahedral phase forms by the peritectic reaction. However, when higher cooling rates are employed, the icosahedral phase directly forms from the undercooled melt. Accordingly, almost single-phase icosahedral structure together with a limited amount of τ-AlCu(Fe) phase is obtained for melt-spun alloys $Al_{65}Cu_{20}Fe_{15}$ and $Al_{62.5}Cu_{25.5}Fe_{12}$. After heat treatment at 750 °C for 3 h, ribbons of $Al_{65}Cu_{20}Fe_{15}$ alloy present a multiphase microstructure consisting of icosahedral, β-AlFe(Cu), λ-$Al_{13}Fe_4$ and τ-AlCu(Fe) phases, while ribbons of $Al_{62.5}Cu_{25.5}Fe_{12}$ alloy present an almost single-phased icosahedral structure [107].

5.2.2. Characteristics of rapidly solidified Al–Cu–Fe alloys

Fig. 11 shows the compositional range for icosahedral microstructure formation in rapidly solidified Al–Cu–Fe alloys. The variation of the copper content of Al–Cu–Fe quasicrystals is somewhat wider than that in thermodynamically stable Al–Cu–Fe quasicrystals. Thus, a broader area for icosahedral quasicrystalline structure generation is obtainable in rapidly solidified Al–Cu–Fe alloys as compared to samples cooled while maintaining thermodynamical conditions. In addition to the wide compositional area for quasicrystalline phase formation, grain growth during the melt-spinning of Al–Cu–Fe alloys is suggested to be very fast. Quasicrystals in the $Al_{65}Cu_{20}Fe_{15}$ alloy have been measured to be 3.5–8.0 μm, which is 7–40 times larger than the grain size in Al–Mn quasicrystals [108].

A high density of structural defects, called phasons, can lead in melt-spun icosahedral Al–Cu–Fe alloys to broadened X-ray diffraction peaks [110–112]. Phasons can be understood as quasicrystalline counterparts of dislocations observed in crystalline materials, with the exception that phasons cannot be clearly seen for example with a transmission electron microscope. Instead, phasons can be perceived as broadened X-ray diffraction peaks or scattered electron diffraction spots. The origin of phasons is discussed in more detail in Section 6.3.

Brand et al. [109] have examined these localised phason defects in an icosahedral $Al_{62}Cu_{25.5}Fe_{12.5}$ alloy. At mod-

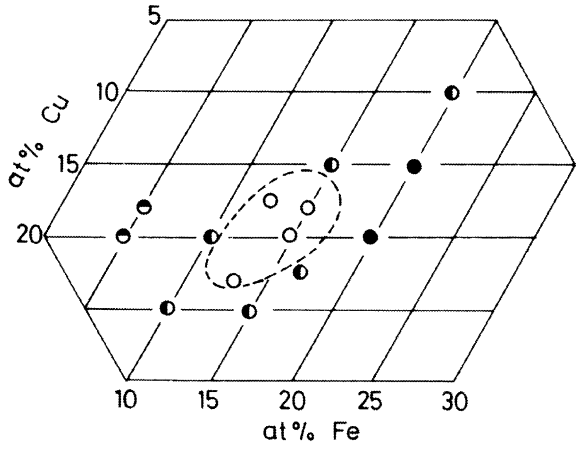

Fig. 11. Compositional range for the formation of icosahedral quasicrystal in rapidly solidified Al–Cu–Fe alloys according to Ref. [108] (○ indicates the presence of quasicrystalline phase only, ◐ presents the coexistence of quasicrystalline and crystalline phases, ◐ shows the simultaneous presence of amorphous and crystalline phases and ● addresses crystalline phases only). Reprinted from Ref. [108], Copyright with permission from Kluwer Academic Publishers.

erate temperatures, these defects become mobile and lead to a short-range atomic motion without involving vacancies [109]. During the annealing of $Al_{65}Cu_{20}Fe_{15}$ alloy, microstructural changes thus occur due to the solute atom repartitioning among quasicrystalline and crystalline phases, which are generally present at least in very small amounts. A diffusionless structural transformation also takes place at moderate temperatures, but its influence is not as remarkable. At higher temperatures, around 650 °C, diffusionless structural changes take place bringing about a completely quasicrystalline icosahedral structure after long-term annealing. The quasicrystalline phase is still stable on annealing at 820 °C, which is $\sim 0.96 \cdot T_m$ of the alloy [110–112]. In turn, the annealing of gas-atomised $Al_{63}Cu_{25}Fe_{12}$ powder with a two-phase structure, consisting of icosahedral phase and the β-AlFe(Cu) phase, similarly produces a purely icosahedral structure on annealing at 700 °C [113]. In contrast to the melt-spun alloy $Al_{65}Cu_{20}Fe_{15}$, the X-ray diffraction peaks measured for $Al_{65}Cu_{22}Fe_{13}$ alloy are observed to be remarkably distorted when annealed around 600 °C, which is attributable to the generation of crystalline approximant phases of quasicrystals [111]. These crystalline approximant phases show structural correspondence to quasicrystals, but they are structurally ordered. Also Jono et al. [114] have observed that the icosahedral quasicrystalline phase in a melt-spun $Al_{63}Cu_{24}Fe_{13}$ alloy was stable at high temperatures but underwent a transformation into crystalline approximant phases via various kinds of intermediate phases at low temperatures. The influence of annealing on the structure of rapidly solidified material, accordingly, is not as sensitive to the preparation method, i.e. whether or not the alloy precedes rapid solidification by melt spinning or gas atomisation, but to its microstructure.

Liu and Köster [115] have analysed in detail the annealing-induced decomposition phenomena of the icosahedral phase in melt-spun Al–Cu–Fe alloys of the compositions $Al_{77}Cu_{13}Fe_{10}$, $Al_{70}Cu_{20}Fe_{10}$, $Al_{65}Cu_{20}Fe_{15}$ and $Al_{60}Cu_{30}Fe_{10}$. They have observed two different decomposition modes of the icosahedral phase. The discontinuous decomposition of the icosahedral phase proceeds by the slow migration of a reaction front into the icosahedral phase. The kinetics of the discontinuous decomposition reactions is mainly controlled by the long-range diffusion (Fig. 12). The discontinuous decomposition can be observed as a peritectoid reaction in $Al_{77}Cu_{13}Fe_{10}$ alloy, as a polymorphic reaction in $Al_{70}Cu_{20}Fe_{10}$ alloy and as precipitation in $Al_{65}Cu_{20}Fe_{15}$ alloy. Continuous decomposition, as observed in $Al_{60}Cu_{30}Fe_{10}$ alloy, proceeds by the development of phason strains inside the icosahedral phase without a definite reaction front. These phason strains yield approximant phases in the structure [115]. These formed crystalline approximant phases are generally of the type of 2/1 and 3/2 rhombohedral approximants. The formation area of the approximant phases in the melt-spun Al–Cu–Fe alloys is shown in Fig. 13 [99,100]. The driving force for

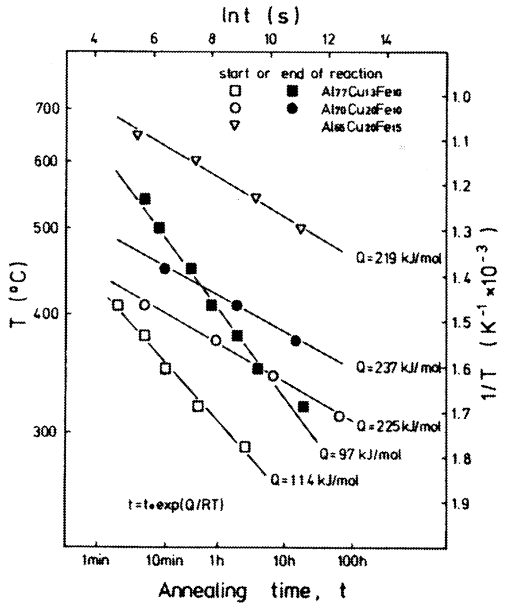

Fig. 12. Kinetics of the discontinuous decomposition of icosahedral phase according to Ref. [115]. Reprinted from Ref. [115], Copyright with permission from Elsevier.

the continuous decomposition phenomena is the minimisation of the system free energy (Fig. 14). The studies of Boudard et al. [116] and Wang et al. [117] have confirmed these decomposition phenomena and their characteristics related to the icosahedral Al–Cu–Fe phase.

It is worth noting that although annealing yields crystalline approximant phases in melt-spun Al–Cu–Fe alloys, no studies have reported their existence after room temperature storage. Thus, the icosahedral phase in the Al–Cu–Fe system seems to be stable under room temperature conditions, even though synthesised by a metastable process. This is, however, not the case for all metastable alloys. For

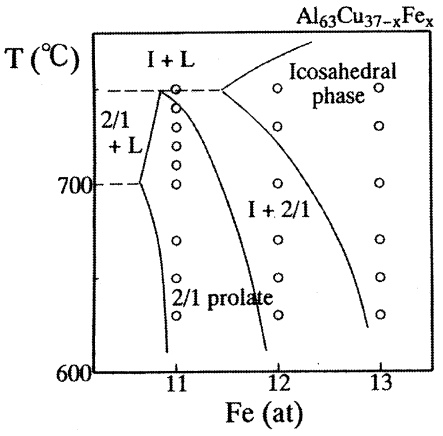

Fig. 13. The approximant phases observed by Waseda et al. in Ref. [100] for the melt-spun Al–Cu–Fe alloys. Reprinted from Ref. [100], Copyright with permission from Elsevier.

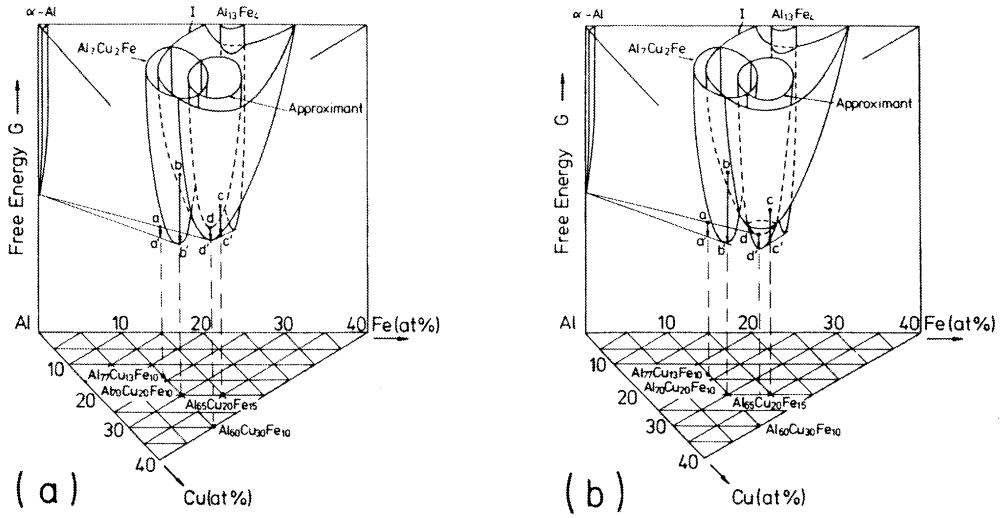

Fig. 14. Hypothetical diagram for the free energy of the different phases in the Al–Cu–Fe system at (a) higher temperatures, e.g. 730 °C, and (b) lower temperatures, e.g. 620 °C, according to Ref. [115]. At higher temperatures the icosahedral phase has a low free energy and is the stable phase, while at lower temperatures the crystalline approximant phases have a free energy lower than that of the icosahedral phase. Reprinted from Ref. [115], Copyright with permission from Elsevier.

example, in melt-spun Al–Mg–Cu alloys, room-temperature storage beyond a period of 3 months results in a microstructural transformation into approximant phases along the grain boundaries of the icosahedral phase [76]. This metastability can sometimes be seen as an advantage, since by promoting the formation of approximant phase nuclei at the grain boundaries for example, strengthening of quasicrystalline Al–Mg–Cu alloys occurs [118]. However, if one wishes to strengthen an aluminium alloy with stable Al–Cu–Fe particles, a casting procedure is needed to form this composite material [119].

5.2.3. *Mechanical alloying of Al–Cu–Fe alloys*

Srinivas et al. [120] have studied icosahedral phase development in a mechanically alloyed $Al_{70}Cu_{20}Fe_{10}$ powder mixture. In a low-energy mill, 40-h milling produces a structure consisting of the icosahedral phase along with the cubic β-AlFe(Cu) phase and a small amount of θ-Al_2Cu intermetallic phase. When milled for 50 h, the intensity ratio of the icosahedral phase to cubic β-phase decreases considerably as compared to the situation after 40-h milling. In the case of high-energy milling, the evolution and disappearance of the icosahedral phase is faster than in the low-energy milling. Srinivas et al. have proposed that the evolution of the icosahedral phase in mechanical milling takes place by a reaction between the β- and θ-phases [120]. The ratio of Al to (Cu+Fe) is suggested to play the most important role in the formation of the icosahedral phase in a milled $Al_{70}Cu_{20}Fe_{10}$ alloy and also in other Al–Cu–Fe alloys. However, the ordering of the icosahedral structure into the face-centered type structure is observed only after heat treatment of $Al_{70}Cu_{20}Fe_{10}$ powders milled for 30 and 40 h [121].

For $Al_{65}Cu_{20}Fe_{15}$ powder mixture, Asahi et al. [122] have shown that only 15 h of mechanical alloying directly introduces the icosahedral structure. Also other research groups have reported the direct synthesis of the icosahedral quasicrystalline phase in the $Al_{65}Cu_{20}Fe_{15}$ powder mixture [121]; Kim et al. [123] have noticed icosahedral phase development after only 10 h of milling. At temperatures above ∼475 °C, the icosahedral quasicrystalline phase is transformed to the ordered face-centered icosahedral phase. High- or low-energy milling for a sufficient time can raise the temperature to this value. For powders milled for 5, 10 or 20 h, formation of the icosahedral phase and its ordering are observed after further heating. The upper limit for the annealing temperature is 858 °C, which is the melting point of the ordered icosahedral structure [122].

Once the $Al_{62.5}Cu_{24.4}Fe_{13}$ powder mixture, compositionally typical for the icosahedral quasicrystalline phase, has been milled, most of the produced structure consists of Al(Cu, Fe) intermetallics, the quasicrystalline phase being a secondary phase. The initial powder charge has, accordingly, been depleted in aluminium. This variation in chemical composition can be compensated for by selecting a powder mixture rich in aluminium. For $Al_{67}Cu_{22}Fe_{11}$, the formation of the quasicrystalline phase proceeds directly by mechanical alloying under intense milling conditions. However, the ordered and stable icosahedral ψ-phase can then be obtained by annealing treatment at 750–780 °C. The formation of the stable and ordered quasicrystalline structure is suggested to be a result of the ordering of metastable intermetallics [124]. This is consistent with the thoughts of Miglierini and Nasu [125].

Mechanical activation has been utilised to successfully synthesise the icosahedral phase in $Al_{64.5}Cu_{24.5}Fe_{11}$ alloy.

However, although attempts to fabricate the icosahedral phase in an $Al_{63}Cu_{25}Fe_{12}$ alloy by mechanical alloying have been made, no signs of icosahedral quasicrystal formation have been noticed [121]. Thus, the critical aluminium content for quasicrystalline phase formation in Al–Cu–Fe alloys lies somewhere between 63 and 64.5 wt.%. In some cases additional alloying by a fourth element has been shown to be beneficial for icosahedral phase formation. For example Cr [126] and Si [123] have broadened the icosahedral phase formation range and, thus, promoted its formation in the Al–Cu–Fe alloy structure.

5.3. Deposition of quasicrystalline Al–Cu–Fe coatings by thermal spraying

Besides straight synthesis of the quasicrystalline phase by rapid solidification of Al–Cu–Fe alloys, further processing of existing rapidly solidified quasicrystalline powders is currently of interest. Research on the thermal spraying of gas-atomised Al–Cu–Fe quasicrystalline powders using the plasma arc spray technique has, however, identified two primary problems. First, the deposited coatings have a tendency towards lower aluminium content than the starting powder due to the higher vapor pressure and easier vaporisation of aluminium compared to copper or iron. This vaporisation is able to move the composition out of the desired icosahedral phase region. Second, the complex peritectic solidification path of the icosahedral phase in an Al–Cu–Fe alloy system may hinder the formation of a purely icosahedral structure. Thus, a tendency to obtain a mixture of metastable crystalline phases along with the quasicrystalline phase in an as-deposited coating exists [127–129]. However, a number of tricks can be used to overcome these problems. To avoid the unwanted vaporisation of aluminium, one possible solution is to use larger feed particles. When heated, larger particles lose a relatively smaller fraction of their aluminium because of the reduced effective surface area. An alternative solution is to start with a powder with a composition slightly higher in aluminium than that desired in the coating. The co-deposition of crystalline phases can be decreased by preheating the substrate material. Also, annealing yields a purely icosahedral structure in the coating [20,128].

Although thermally sprayed quasicrystalline Al–Cu–Fe coatings are primarily deposited by plasma spraying, other thermal spraying techniques for coating preparation are of current interest. At present, the greatest challenge seems to be the adjustment of spraying parameters so that the quasicrystalline phase in the spray powder does not decompose during the spraying process.

6. Properties of Al–Cu–Fe quasicrystals

Previous sections discussed how the structure of quasicrystals differs remarkably from that of crystalline materials. The same applies to their properties. In this chapter the unique physical qualities, surface behavior characteristics and mechanical properties of quasicrystals and especially Al–Cu–Fe quasicrystals are reviewed.

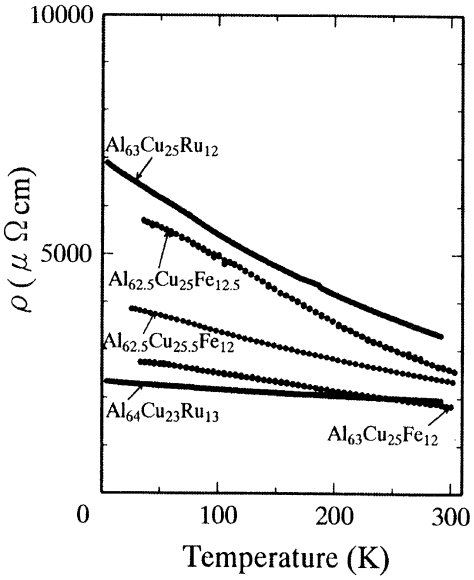

Fig. 15. The temperature dependencies of electrical resistivities ρ of Al–Cu–Fe and Al–Cu–Ru quasicrystalline phases according to Ref. [134]. Reprinted from Ref. [134], Copyright with permission from Elsevier.

6.1. Physical properties of Al–Cu–Fe quasicrystals

Quasicrystals probably differ most from their crystalline counterparts with regard to electronic properties [24]. The electrical resistivity ρ is generally large for quasicrystals, yielding poor electrical conductivities [130,131], while the electrical conductivities of crystalline metallic alloys are high. Berger et al. have measured the electrical conductivity of icosahedral Al–Cu–Fe, Al–Pd–Mn and Al–Pd–Re and categorised it in the same range as for doped semiconductors [132]. However, huge differences exist between the electrical conductivity properties of different quasicrystals. For Al–Mn quasicrystals, values as high as 800–1000 μΩ cm for electrical resistivity have been measured at room temperature. However, Al–Mn has a small negative temperature coefficient; resistivity values for quasicrystalline Al–Mn alloys increase with decreasing temperature in the low temperature region [130]. A negative and linear temperature-dependence is typical for many quasicrystalline alloys, and is also suggested for the conductivity of Al–Cu–Fe and Al–Cu–Ru quasicrystals at temperatures above −243 °C [133,134]. The temperature dependencies of these quasicrystals are portrayed in Fig. 15. For quasicrystalline Al–V alloy the electrical resistivity is nearly constant in the low temperature region, whereas for quasicrystalline Al–Mn–Si alloy, a positive temperature coefficient is measured, as is typical for most usual metals [130].

Bilušic et al. have shown that the electrical conductivities of icosahedral Al–Cu–Fe alloys of compositions $Al_{62}Cu_{25.5}Fe_{12.5}$ and $Al_{63}Cu_{25}Fe_{12}$ become higher with increasing temperature, reaching $35{\cdot}10^3\ \Omega^{-1}\ m^{-1}$. However, the electrical conductivity of the sample with 12.5% Fe is lower than that of the sample with 12% Fe. This is due to the fact that a structure closer to the perfect icosahedral structure means a smaller number of free carriers and, consequently, lower electric conductivity [135]. This is also admitted by other research groups [131].

The electronic structure of materials seems to be strongly related to their electronic properties. Crystalline materials with high electrical conductivity generally contain free electrons; electrons are not tightly bound in their places but can roam freely and conduct electricity. In insulating materials, the electrons are tightly bound to their places and cannot conduct electricity [136]. In quasicrystals and semiconductors, in contrast, a gap exist in the density of electron states, meaning conduction of some sort. The closer the quasicrystalline structure is to a perfect quasicrystalline structure with no structural defects, phasons, the higher the electrical resistivity of the material. Thus, the high electrical resistivity observed in quasicrystals is associated with the gap observed in the conduction band [137]. Nevertheless, although generally and most widely accepted, the electron band gap model is not the only theory suggested for the peculiar electrical behavior of quasicrystals. The weak localisation [134], the electron–electron interaction theories [134,138], the quantum interference effects [131,138], as well as the very low Al 3p density of electron states and the vanishing of Al p conduction band [139], have also received some support. Thus, no definite consensus has been obtained as to the reason for the unique electrical properties of quasicrystals as compared to crystalline or amorphous materials.

Similarly as for electrical resistance, the magnetoresistance of quasicrystals is anomalously large at low temperatures. The same behavior has earlier been attributed to amorphous metals [131]. In icosahedral quasicrystals in alloy $Al_{65}Cu_{20}Fe_{15}$, no traces of magnetic behavior can be found [125]. Often, quasicrystals do not show even paramagnetism [133]. However, $Al_{65}Cu_{20}Fe_{15}$ remains paramagnetic down to 8 K (−265 °C).

In addition to electrical conductivity, the optical conductivity of quasicrystalline materials, in general, is very different to that for metallic behavior. Optical conductivity refers to the frequency dependence of the electrical conductivity. For most quasicrystalline materials, optical conductivity remains small for most of the frequency range, especially towards low-energy values. Nevertheless, a rather strong resonance shows up at around $10^4\ cm^{-1}$ or 290 THz corresponding to infrared radiation with a wavelength of ∼1 mm [133]. In contrast, the optical conductivity of Al–Cu–Fe quasicrystals is reported to be noteworthy throughout the frequency scale, increasing linearly with increasing frequency [131]. This property can be made use of in selective absorber applications. Al–Cu–Fe thin films with a mixture of crystalline and quasicrystalline phases are especially suitable for these purposes. Very thin quasicrystalline films of composition $Al_{62}Cu_{25}Fe_{12}$ and with thicknesses ranging from 10 to 13 nm have been produced with stacks of crystalline Al_2O_3 antireflective coatings on copper; these surfaces show a high solar absorbance of 90% and a low thermal emittance. The optical constants of these $Al_{62}Cu_{25}Fe_{12}$ films, $1300–1700 \pm 250{\cdot}10^{-8}\ \Omega m$, seem to be quite close to those of high quality quasicrystalline samples, $3000{\cdot}10^{-8}\ \Omega m$ [140].

The thermal conductivity of quasicrystals is generally extremely low, much lower than that of crystalline metallic materials and similar to that of oxides, which are known as very efficient insulators. Although the thermal conductivity of quasicrystals somewhat increases with temperature, it remains very low throughout the whole temperature range from room temperature to 800 °C [141]. As regards the low temperature region, Bilušic et al. [135,142] have studied the thermal conductivities of $Al_{62}Cu_{25.5}Fe_{12.5}$ and $Al_{63}Cu_{25}Fe_{12}$ alloys and found them identical. At very low temperatures, in the temperature range from 0.1 to 6 K (−272.9 to −267 °C), the phonon thermal conductivity first shows a $T^{2.7}$ dependence with temperature, then a linear increase, and up to 6 K (−267 °C) a much more rapid dependency than T^3 is observed [143]. From this temperature on, the phonon thermal conductivity of $Al_{62}Cu_{25.5}Fe_{12.5}$ and $Al_{63}Cu_{25}Fe_{12}$ alloys increases monotonically with temperature showing a shallow maximum at ∼23 K (−250 °C) as a consequence of structural scattering of lattice vibrations typical for icosahedral quasicrystals. This maximum is followed by a minimum around 73 K (−200 °C), and a subsequent increase. This increase is related to the activation of localised phonon sites [135,142].

The linear thermal expansion of quasicrystals is rather high. It is similar to that of iron and steel but lower than that of aluminium [141]. According to Korsunsky et al. [144], quasilattice defects of phason type contribute to the increased thermal expansivity of quasicrystals. The phason-type defects introduce atomic arrangement disorder into the lattice; inter-atomic distances are increased and bond forces correspondingly decreased so that thermal expansion occurs with greater ease. Due to this special role of phason defects, melt-spun Al–Cu–Fe alloys showing high phason intensity have superior linear thermal expansion compared to quasicrystalline Al–Cu–Fe alloys prepared by other methods. However, the high thermal expansion may cause trouble during joining operations of quasicrystalline Al–Cu–Fe alloy parts or even during thermal coating procedures on substrates exhibiting totally different thermal expansion behavior.

6.2. Surface characteristics of Al–Cu–Fe quasicrystals

For clean quasicrystalline surfaces, the quasiperiodicity is retained at the surfaces. The surfaces consist of rather flat

terraces separated by crooked steps, as customary for crystalline surfaces [40]. Cai et al. [145] have further studied the surface structure of Al–Cu–Fe quasicrystals. The surface is bulk-terminated with a bulk-like layer-dependent composition. Surface tends to form between different groups of closely spaced planes. The grouped planes can be sorted into three sets, with three, five and nine planes. These plane groups correspond to step heights of 2.5, 4.0 and 6.5 Å, respectively. The groups of planes are separated by distances ranging from 1.4 to 1.6 Å with no atoms in between. Thus, the quasicrystalline order is maintained well within the favored groups of planes, where atoms interconnect densely throughout the structure, but less well between the groups of planes [145]. Also Jenks and Thiel have observed that the chemical bonds inside the icosahedral atomic clusters are strong while the intercluster bonds are weaker [40]. It is also interesting that, compared to the surface structure of quasicrystalline Al–Pd–Mn, the surface of quasicrystalline Al–Cu–Fe contains screw dislocations and pentagonal pits, neither of which has been observed on Al–Pd–Mn. However, the surface in both cases is rich in aluminium. Also, the observed step heights are very comparable [145]. Of course, the surface structure of quasicrystalline materials depends strongly on how the surface is prepared. For example, a cleaved surface is significantly rougher than a sputter-annealed surface [40].

The surface energies of quasicrystals, especially Al–Cu–Fe quasicrystals, are rather low. In terms of contact angle measurements, the quasicrystalline surfaces behave more like covalently-bound materials than like metals [40]. The surface energy of quasicrystals is somewhere between that of stainless steel and Teflon, but much closer to Teflon as soon as their lattice quality, phase purity and surface preparation are adequate. The best quasicrystals exhibit surface energies only 25–30% above that of Teflon [70]. Belin-Ferré et al. [56] have correlated this low surface energy to the low Al 3p density of states, i.e. to the low number of nearly-free electrons available for bonding with interacting molecules such as water. Of quasicrystals, icosahedral quasicrystals exhibit the lowest adhesion energy of water due to these special structural characteristics [56]. Also for melt metals such as tin, very low contact angles have been measured at the surface of Al–Cu–Fe quasicrystals [146].

The low surface energy of quasicrystals is reflected in their low coefficient of friction. The coefficient of friction remains essentially low for Al–Cu–Fe quasicrystals [113]. Their surface friction properties are equivalent to those of the hardest materials, as demonstrated in Fig. 16. According to Zhang et al. [147], the friction coefficients of Al–Cu–Fe quasicrystalline phase and its crystalline approximants are one third of that of commercial low carbon steel, the friction coefficients being 0.12, 0.14 and 0.4, respectively [147]. However, the low friction coefficient is not solely related to the high values of hardness and Young's modulus of quasicrystals but primarily to the reduced electronic interactions of the surface. If crystalline phases are present, they strongly

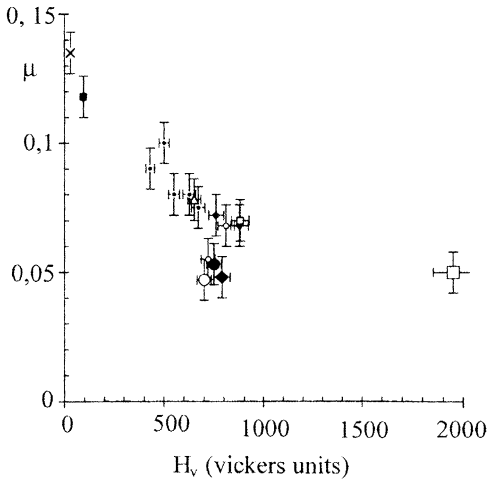

Fig. 16. Friction coefficient μ measured in Ref. [70] in an alternating sliding scratch test with a diamond indenter for a number of specimens with variable hardness. Symbols are as follows: ○, twinned icosahedral quasicrystal $Al_{70.5}Pd_{21}Mn_{8.5}$; large ●, sintered $Al_{70}Pd_{20}Mn_{10}$; small ○, tetragonal ω-$Al_{70}Cu_{20}Fe_{10}$, orthorhombic O1-$Al_{71.2}Cu_{9.8}Fe_{8.5}Cr_{11}$ and monoclinic λ-$Al_{73.5}Cu_3Fe_{23.5}$ ($Al_{13}Fe_4$-type); small ●, Al-CuFe β-cubic CsCl-type ($\leq$5% in volume); small ◆, sintered Al-CuFe icosahedral+β-cubic; large ◆, sintered single-phase icosahedral $Al_{59}B_3Cu_{25.5}Fe_{12.5}$; ×, f.c.c.-Al; large □, sintered cubic alumina; small □, hard Cr-steel; ■, f.c.c.-Cu; △, window glass. Reprinted from Ref. [70], Copyright with permission from Elsevier.

increase the friction coefficient. Only 5% β-AlFe(Cu) cubic phase in quasicrystalline base structure in $Al_{62}Cu_{25.5}Fe_{12.5}$ alloy is needed to double the friction coefficient of the purely icosahedrally structured $Al_{62}Cu_{25.5}Fe_{12.5}$ alloy [70,71].

The friction measurements of quasicrystalline materials, however, pose some experimental problems. First, the friction partner, the third partner, i.e. the lubricant, wear debris or transfer layer, and testing conditions contribute to the overall friction response [133], and are not always reported properly, which also applies to the used testing indenters and tips. The best results, i.e. the lowest friction coefficients, are generally achieved with a very thin tip.

In oxide-containing environment, aluminium-rich quasicrystals tend to passivate by forming a thin, protective layer of aluminium oxide independently of the surface preparation method [40]. Popović et al. [148] propose that Al–Pd–Mn quasicrystals form a layer-by-layer surface composition, of which the topmost layer is aluminium-rich and therefore aluminium is the first element to oxidise. The diffusivities of the alloying elements in the quasicrystal are much smaller than in the elemental samples and so the topmost layer composition determines which elements are oxidised. Accordingly, selective oxidation of the elements in the alloy takes place [148]. Oxidation in more humid environments or at higher temperatures can result in the build-up of thicker oxide layers and attacks on other elements. Also, oxidation can move the surface and near-surface composition out of the field of quasicrystalline stability, giving rise to surface structure transformations [40].

In an Al–Cu–Fe alloy of the composition of $Al_{63}Cu_{25}Fe_{12}$, oxidation of icosahedral phase first causes dissolution of the grain boundaries, while the inner surface of the grains oxidises into α-Al_2O_3. This oxidation of the grain surfaces is observed to start by oxide island formation accompanied by icosahedral phase transformation into the λ-$Al_{13}Fe_4$ phase. Thus, a loss of copper is to be expected. Finally, the formation of γ-Al_2O_3 takes place on the remaining icosahedral phase surface as well as on the surface of the λ-$Al_{13}Fe_4$ phase. Oxidation is also found to induce a phase transformation of the icosahedral phase into the β-AlFe(Cu) phase. However, no evidence of a continuous phase transformation due to the diffusion of oxygen into the quasicrystals has yet been found [149].

As for the high-temperature oxidation of Al–Cu–Fe quasicrystals, a parabolic rate constant for the oxidation of Al–Cu–Fe quasicrystals has been measured. The oxidation behavior is strongly determined by the copper content of the quasicrystals. Copper triggers the indirect transformation of θ-Al_2O_3 into α-Al_2O_3 [150], a reaction which has not been observed to occur at lower temperatures. Thus, this relation between the copper content of the material and the oxide layer composition has not been observed for room-temperature oxidation. In contrast, in acidic and basic solutions, copper again plays the key role. Dissolution of aluminium and iron from $Al_{63}Cu_{25}Fe_{12}$ has been observed, leaving the porous copper layer and a destabilised icosahedral structure behind. This destabilised icosahedral structure undergoes partial transformation into the β-AlFe(Cu) phase [151–153]. The same destabilisation of the icosahedral structure occurs as a result of contamination of the $Al_{62}Cu_{26}Fe_{12}$ surface for example by carbon [154,155]. After a salt spray test, enrichment of both aluminium- and copper-rich oxide layers and hydroxide layers occurs at the surface, protecting the underlying quasicrystalline structure [151–153]. To sum up, there is no evidence for improvement in corrosion resistance due to the presence of the quasicrystalline structure. The quasicrystalline structure behaves as any Al–Cu–Fe structure in corrosive environments, the corrosion behavior of the alloy being the sum of the corrosion behaviours of the individual elements of the alloy. However, biocompability is observed in quasicrystalline materials, which is not very general in crystalline metallic alloys [133].

In contrast to the oxidation of quasicrystalline materials, hydrogenation has not been proved to cause transformation of the quasicrystalline phase into crystalline counterparts. In the alloy $Zr_{69.5}Ni_{12}Cu_{11}Al_{7.5}$, for example, hydrogenation is found to raise the quasilattice constant by ∼10% at the hydrogen-to-metal ratio of 1.9. During annealing, the hydrogen is driven out prior to any other reaction. Due to this property, Zr–Ni–Cu–Al and Ti–Zr–Ni quasicrystals show promise for hydrogen-storage applications [156]. No such powerful effect, however, has been observed in quasicrystalline Al–Cu–Fe alloys.

The wear resistance of quasicrystals strongly depends on their hardness and brittleness. Thermally sprayed Al–Cu–Fe coatings composed of only quasicrystalline phase exhibit quite good abrasive wear resistance due to their high room-temperature hardness. However, the room-temperature brittleness impairs abrasive wear behavior. The addition of only very small amounts of Fe–Al into Al–Cu–Fe can cause a transition in the abrasive wear mode from brittle fracture to plastic flow [157]. Generally, crystalline phases are present in coating structures in small amounts and cause the abrasive wear of Al–Cu–Fe quasicrystalline coatings to occur via plastic flow and delamination [113,158]. The same applies to high-temperature conditions. When plastic deformation occurs, the hardness values are decreased. Consequently, less good abrasive wear resistance is obtained. Thus, a compromise between reasonable hardness and degree of plasticity yields good abrasive wear resistance to quasicrystalline Al–Cu–Fe alloys. The hardness behavior as well as the ductility of Al–Cu–Fe quasicrystals are discussed more in detail in the next section.

6.3. Mechanical properties of Al–Cu–Fe quasicrystals

Dislocations play a key role as regards the mechanical properties of crystalline materials. They mediate the plastic flow and cause a strain field in one direction, thereby influencing the ductility and strength as well as the work hardening behavior. Similarly to crystals, dislocations in quasicrystals are important for their mechanical properties. However, dislocations in quasicrystals are special in that they are accompanied by strain fields in two directions. The 'conventional' elastic strain takes place in a real space $E_{||}$, while the phason strain occurs in a perpendicular space $E_{\perp}$. Based on the existence of this phason strain, the characteristic features of dislocations in quasicrystals are somewhat different from those in crystals. Still, a perfect dislocation in quasicrystal is a line defect vector in the physical but high-dimensional space (Fig. 17). In icosahedral quasicrystals, the Burgers vector of most dislocations is parallel to a two-fold direction, the close-packed five-fold or two-fold planes operating as glide planes [159].

The Burgers vector b of a dislocation in a quasicrystal consists of two components: a component parallel to the real space ($b_{||}$) and a component parallel to the perpendicular space ($b_{\perp}$). The parallel component yields a phonon strain field around the dislocation as in crystals, whereas the perpendicular component corresponds to a phason strain field. The direction of the Burgers vector b can be determined by the invisibility condition $g \cdot b = 0$, as in crystals. However, the invisibility condition extends also into the phason space. Thus, the invisibility condition is generalised to $G \cdot B = g_{||} \cdot b_{||} + g_{\perp} \cdot b_{\perp} = 0$. There are, accordingly, two cases in which this invisibility condition is satisfied. The 'strong' invisibility condition is the case $g_{||} \cdot b_{||} = g_{\perp} \cdot b_{\perp} = 0$, where $g_{||} \cdot b_{||} = 0$ is the same as the invisibility condition for crystals. The 'weak' invisibility condition is $g_{||} \cdot b_{||} = -g_{\perp} \cdot b_{\perp} \neq 0$. This weak invisibility condition is characteristic of dislocations in quasicrystals [160].

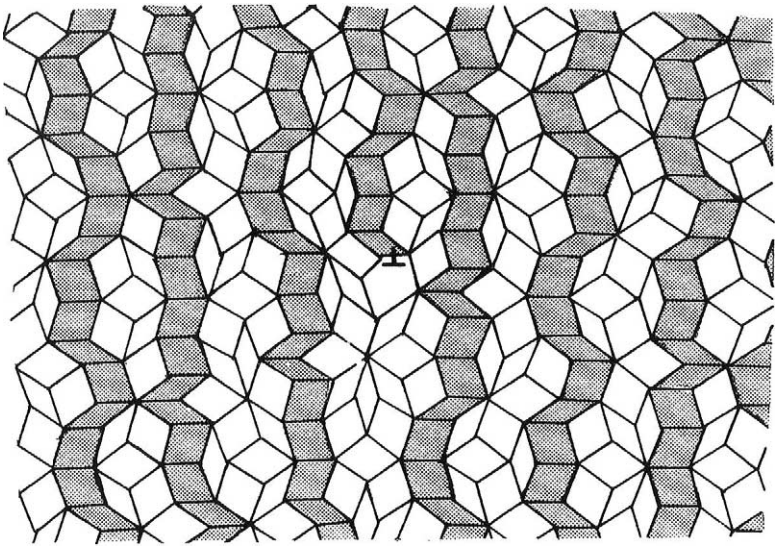

Fig. 17. A perfect edge dislocation in the two-dimensional Penrose lattice after Ref. [162]. Lattice planes consisting of parallel-sided tiles are shaded to show the strain-field. Reprinted from Ref. [162], Copyright with permission from Elsevier.

In addition, as the structure of quasicrystals is not periodic, the lattice areas above and below the glide plane behind a moving dislocation do not match in general. This mismatch of the lattice across the glide plane is called a matching-rule violation and can be observed with a transmission electron microscope as a planar-fault contrast appearing and then vanishing [159]. The previously mentioned invisibility of phason defects in the case of melt spun Al–Cu–Fe alloys refers to this phenomenon.

Similarly to crystalline materials, dislocations in quasicrystals mediate the plastic flow [159,161]. The characteristics of dislocation in quasicrystals are, accordingly, reflected in the ductility, strength and the work hardening behavior, identically to crystals. In quasicrystalline materials, the high-energy phason faults make the dislocations immobile in the low temperature range where atomic diffusion is not allowed, leading to brittle fracture [162,163]. Brittle fracture usually occurs by an intergranular process [164]. Quasicrystals behave, consequently, like any intermetallic compound at room temperature and intermediate temperatures, being very brittle. Köster et al. [165] have compared the deformation characteristics of quasicrystalline and crystalline phases in the ternary Al–Cu–Fe alloys. These characteristics are summarised in Table 4. Tei et al. [166] have further concluded that the icosahedral phase of a simple-metal system is similar to its crystalline intermetallic counterparts as regards elastic properties.

At elevated temperatures quasicrystalline materials become plastic [167]. Dislocation motion is proposed to be one important mechanism for the high-temperature plastic deformation of Al–Cu–Fe quasicrystals [34,168,169]. According to Shield and Kramer [170], this dislocation glide takes place predominantly at grain boundaries in the temperature range 680–720 °C. Besides dislocation motion, atomic diffusion is suggested to be the major cause of deformation causing atomic transport at large distances [164]. Twinning is observed to occur in Al–Cu–Fe quasicrystals without [171] and with high-temperature deformation [172]. Yet, whatever the deformation mechanism at high temperatures, Young's modulus decreases progressively and a ductile regime

Table 4
Compositions and mechanical properties of crystalline and quasicrystalline phases in ternary alloy system Al–Cu–Fe according to Ref. [165]

Composition	Phases	Structure	Hardness (HV 0.25 N)	Toughness K_{IC}, MPa $(m)^{1/2}$	Brittle-to-ductile temperature, °C
$Al_{72}Fe_{28}$	Al_5Fe_2	Orthorhombic	1100	1.05	∼550
$Al_{75.5}Fe_{24.5}$	$Al_{13}Fe_4$	Monoclinic	1070	1.03	∼750
$Al_{67.6}Cu_{32.4}$	Al_2Cu	Tetragonal	595	1.14	∼400
$Al_{48}Fe_{52}$	AlFe(Cu)	Cubic (CsCl type)	775	>20	∼430
$Al_{63}Cu_{25}Fe_{12}$	ψ-AlCuFe	Icosahedral	1000	1.64	∼650

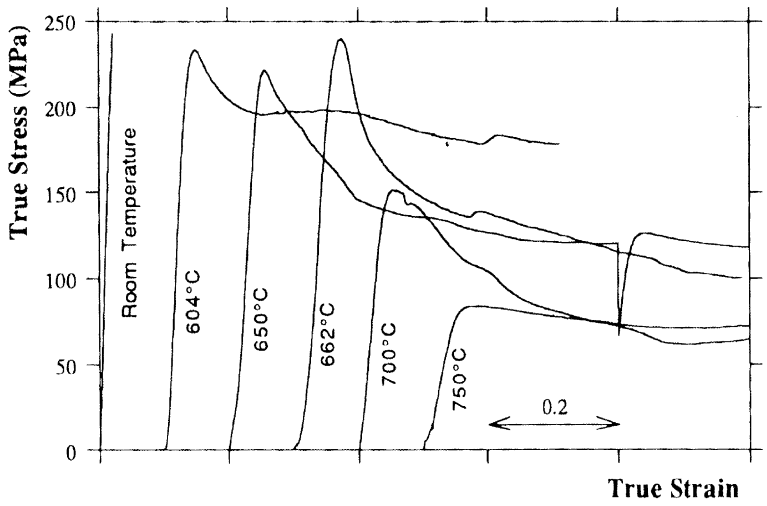

Fig. 18. True stress–strain curves of Al–Cu–Fe quasicrystalline alloy in the temperature range from room temperature to 750 °C after Ref. [164]. Reprinted from Ref. [164], Copyright with permission from Elsevier.

appears with an increasingly homogeneous deformation mode. Starting from 650 °C, the plasticity becomes totally homogeneous and the total deformation may reach very high values up to 130% [163,164].

As the elastic properties of Al–Cu–Fe quasicrystals are comparable to their crystalline counterparts, their yield strength should also be nearly equal. However, with increasing strain their mutual behavior differs somewhat. In contrast to metallic materials, where the lattice structure is restored after a dislocation has passed, dislocation motion in quasicrystals produces a tail of matching-rule violations [167,173]. Since these matching-rule violations are structural and chemical disorders, the ideal structure of the quasicrystals is destroyed step by step. This results in a decreasing stress value, i.e. deformation softening, as a result of increasing strain [167], while deformation hardening generally takes place in crystalline metals. At low temperatures, the maximum stress of Al–Cu–Fe icosahedral phase reaches a value of 250 ± 15 MPa [164]. This value is very low even as compared to the ultimate tensile strength values of other Al–Fe-based quasicrystalline materials, of which the best is 660 MPa for Cr- and Ti-containing alloy [174]. The stress–strain curves of Al–Cu–Fe quasicrystalline alloy at different temperatures are shown in Fig. 18. No deformation hardening occurs even at higher temperatures. Furthermore, although the maximum stress levels of icosahedral Al–Cu–Fe alloys are low at room and intermediate temperatures, they further decrease with increasing temperature.

Giacometti et al. [175,176] have studied the creep behavior of quasicrystalline $Al_{63.5}Cu_{24}Fe_{12.5}$ alloy. They have obtained different creep responses that depend not only on the temperature and stress level at which they were performed, but also on the past deformation history of the specimens. The creep curves at low stress levels exhibit only one stage of continuous creep rate decrease. At higher stress levels, this primary stage is followed by a region of accelerated creep rate, which is not associated with creep damage but represents an intrinsic property of Al–Cu–Fe quasicrystals. Dislocations are involved in the entire creep process, as in crystalline materials.

The microhardness behavior of quasicrystalline Al–Cu–Fe alloys may be correlated with the brittle-to-ductile transition temperature evidenced through conventional mechanical testing. The microhardness of Al–Cu–Fe quasicrystalline alloys as a function of temperature is shown in Fig. 19. The microhardness values of Al–Cu–Fe quasicrystals are very high and almost constant at ambient and intermediate temperatures corresponding to the brittle regime. Audebert et al.

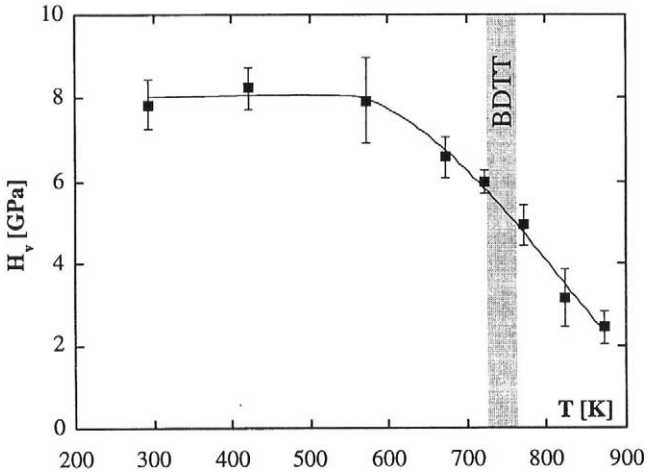

Fig. 19. Vickers microhardness of Al–Cu–Fe quasicrystalline alloy as a function of temperature. The brittle-to-ductile transformation temperature is also shown in the figure. Reprinted from Ref. [177], Copyright with permission from Elsevier.

Table 5
Chemical compositions and microhardness values of quasicrystalline coatings studied by Audebert et al. [126]

Composition (at.%)	$Al_{64.5}Cu_{24.5}Fe_{11}$	$Al_{77}Cu_6Fe_8Cr_9$	$Al_{77.5}Fe_{12}Cr_{10.5}$	$Al_{84}Cr_{16}$
$HV_{0.2}$	725 ± 50	720 ± 20	655 ± 50	465 ± 50

[126] have compared the room-temperature microhardness values of four different aluminium-based quasicrystalline coatings. The composition and microhardness of these coatings are summarised in Table 5. Of these alloys, Al–Cu–Fe presents the highest microhardness as well as the greatest brittleness and highest susceptibility to crack formation [126]. The microhardness values of Al–Cu–Fe quasicrystals sharply decrease when higher temperatures are reached corresponding to the ductile regime. These same principles apply to macrohardness values [24,113,159,167]. Intragranular cracks may be seen around Vickers microindentations performed in the brittle regime, while intergranular cracks are dominant in the ductile regime [177]. Besides the formation of intragranular cracks, occasional microstructural transformation of the quasicrystalline phase into crystalline counterparts has been observed during microhardness testing of quasicrystalline Al–Cu–Fe alloy [178], although the icosahedral phase is known to be extremely stable under compression [179].

6.4. Properties and microstructure of quasicrystalline alloys: a comparison with crystalline counterparts

In general, the microstructure and properties of materials are interconnected. As a group, metallic crystalline materials give rise to certain properties, which do not occur, for example, in amorphous glasses, such as good electrical and thermal conductivity and work hardening. Quasicrystalline metallic alloys show an interesting structural combination. They are composed of metallic elements and they obey a structure close to crystalline, but not perfectly satisfying the definition of crystallinity. Thus, the atoms are not ordered into unit cells but in clusters, while the electrons inside the atoms do not form a continuous conducting band but show a band gap. These special microstructural features result in a combination of properties, which cannot currently be provided by any other material group.

In quasicrystalline alloys, the band gap in the density of electron states mostly influences the physical properties of these materials. First, the electrons do not conduct electricity or heat very well due to the discontinuous electron conduction band. In Al–Cu–Fe quasicrystals, the electron band gap is extremely deep. However, as electrons still exist, a conduction of some sort exists, making quasicrystalline alloys poor electrical and thermal conductors, but not insulators. In crystalline metal alloys, in contrast, where electrical and thermal conduction usually is very good, a continuous conduction band exists. The extremely low electronic conductivity of Al–Cu–Fe quasicrystals is also reflected in their high optical conductivity. Second, the electron structure of quasicrystalline alloys leads to the absence of magnetism. In quasicrystalline Al–Cu–Fe alloys, most atoms are either Al or Cu atoms, both of them having only one electron in the outermost electron shell, thus giving rise to a non-existent resultant angular momentum yielding magnetism. This also applies to crystalline Al and Cu atoms. Fe atoms, in turn, show magnetism, but adopt a minor role in Al–Cu–Fe quasicrystalline alloys. In quasicrystalline Al–Cu–Fe alloys, the band gap in the electron density of states further militates against magnetism. Since some magnetic momentum still exists in the electron structure of Al–Cu–Fe quasicrystals, they show paramagnetism. Besides the physical properties, some chemical or surface properties may be linked to the electron structure of Al–Cu–Fe quasicrystals. Third, the reduced electronic interactions due to the band gap in the electron density of states leads to low surface energy and coefficient of friction for quasicrystalline Al–Cu–Fe alloys. In crystalline counterparts with a continuous conducting band, electronic interactions are greater in number, bringing about higher values for surface energy and coefficient of friction. The biocompatibility of quasicrystalline alloys is suggested to be the result of reduced electronic interactions as well.

The atom structure of quasicrystalline alloys is linked to a variety of properties, including physical and mechanical properties and surface characteristics. The grouping of atoms to form clusters, the connection of the clusters via oriented bonds to form an aperiodic structure and a stepped surface structure are the most important details of atomic structure to influence these properties. First of all, the thermal expansion of quasicrystalline Al–Cu–Fe alloys very much resembles that of crystalline materials. In both structures, the atoms inside atom clusters or unit cells may move somewhat freely despite their exactly defined positions, allowing an increase in the average distance between the atoms. Second, the aperiodicity in atomic order is responsible for the brittleness, low strength values and high hardness of quasicrystalline materials. As the movement of dislocations generally is associated with the ductility and strength of materials, the local disorder they leave behind in quasicrystalline materials also does so, but by impairing them. Therefore, strains in quasicrystals are low, easily leading to brittle fracture. In addition, work softening is related to the increased structural disorder, and high hardness values, in turn, are linked to the brittleness of material. Third, the similarity of corrosion behavior of quasicrystalline Al–Cu–Fe alloys and

their crystalline counterparts arises as a consequence of their identical surface structures. The surface structure of both quasicrystalline and crystalline alloys consists of flat terraces separated by crooked steps. Based on this structural likeness, there is no difference in their corrosion behavior. However, the quasicrystalline surfaces have been found to be enriched in aluminium, thereby favoring the formation of an aluminium oxide layer. This kind of selective oxidation is not a basic rule in crystalline materials.

7. Current and potential applications of Al–Cu–Fe quasicrystals

The unusual electrical and thermal properties of quasicrystalline alloys can be employed in catalyst applications. The fact that several of the quasicrystalline alloys discovered contain catalytically important constituents further supports this scenario [2]. Quasicrystalline Al–Cu–Fe alloys have the potential to be used especially as a catalyst for steam-reforming of methanol. It is even expected that these quasicrystalline Al–Cu–Fe catalysts will appear on the market in the near future [153]. Besides chemical catalysis, the electrical and thermal properties of quasicrystalline alloys may become useful for thermopower generation [70,180]. Materials in these thermoelectric applications, for example in refrigeration and power generation, should have low thermal conductivity, quite high electrical conductivity and high thermopower, which is a product of several electrical and thermal quantities. In general, quasicrystals seem to meet these requirements of good thermoelectric materials. However, the electrical conductivity of Al–Cu–Fe quasicrystals is too low to be used in these applications due to their deep band gap. Al–Cu–Fe quasicrystals can, however, be used in thermometry and heat flow detection due to their temperature-dependent electrical conductivity; the development of such devices is under way [133].

Other possible applications of quasicrystalline Al–Cu–Fe alloys include light absorption. The design of selective quasicrystalline light absorbers takes advantage of the specific optical properties of quasicrystals [70]. Al–Cu–Fe quasicrystalline thin films are especially well suited as selective absorbers in solar thermal applications due to their good solar absorbance of 90% and good optical properties. This kind of solar absorbance panel exploiting quasicrystalline Al–Cu–Fe layers has already been fabricated [140]. Besides solar cells, insulator screen and window glass applications could make use of the optical properties of Al–Cu–Fe quasicrystals [133]. Other potential applications of the optical properties of Al–Cu–Fe quasicrystals comprise bolometers in the detection of infrared radiation.

The complete absence of work hardening, in strong contrast to metallic alloys, is one of the most interesting properties of quasicrystals [24]. Besides the work softening behavior, the high hardness and good wear resistance accompanied by the low friction coefficient of Al–Cu–Fe and other quasicrystals advocates their use as a coating material. Accordingly, a commercial application of quasicrystals has emerged, which seeks to take advantage of the unique mechanical, thermal and surface properties of these materials. The product is a cookware surface coating named Cybernox®. The coating is an Al–Cu–Fe–Cr alloy deposited as a thin coating by thermal spraying techniques [181]. Also pure Al–Cu–Fe and alloyed Al–Cu–Fe–Si quasicrystals can be used for the same purpose, since neither contains toxic elements. The low coefficient of friction and high hardness can also be made use of in cylinder liners and piston coatings in motorcar engines [133].

In addition to low- and moderate-temperature wear protection applications, quasicrystalline Al–Cu–Fe alloys could be subjected to high-temperature use against wear. The work softening of Al–Cu–Fe quasicrystals and their improved ductility properties at temperatures above 600 °C support their use as thermal barrier coatings. Furthermore, the poor thermal conductivity of Al–Cu–Fe quasicrystals supports applications of this type. The melting temperature of Al–Cu–Fe quasicrystals is ∼860 °C, which sets the upmost limit for the high-temperature applications. The formation of a protecting aluminium oxide layer on the surface of Al–Cu–Fe quasicrystals in mildly oxidising environments supports their use in many corrosion-protection coating applications in addition to those in wear protection technology. The biocompatibility together with the good surface properties is a very promising property combination for introducing quasicrystals into surgical applications as a coating on metallic parts used for bone repair and prostheses [133].

8. Conclusions

Quasicrystals are new materials that have the potential to be used in many areas of advanced technology. In this paper, the microstructure, fabrication and properties of quasicrystalline Al–Cu–Fe alloys were reviewed from the standpoint of the materials engineer, focusing on those areas of greatest importance for future applications of Al–Cu–Fe quasicrystalline materials. As a result, emphasis was placed on describing the basic differences between crystalline and quasicrystalline materials with respect to structure and properties. The special structural features of Al–Cu–Fe quasicrystalline alloys were clarified. Much was said about the production methods of quasicrystalline materials and their application to Al–Cu–Fe quasicrystalline alloys. The characteristics of these production methods were compared in order to provide the reader with the information necessary for choosing a proper fabrication technique for quasicrystals in certain applications. Finally current and possible future

applications of Al–Cu–Fe quasicrystals in the light of their properties were illustrated.

After the two decades of quasicrystal research, quasicrystals have found their place in the structural classification of materials. Today, they are regarded as crystalline materials, since they show peaks in X-ray data and points in electron diffraction patterns. However, quasicrystals still have their planes assembled aperiodically due to the orientation of atom clusters with respect to each other. Based on this crystallinity, analysis of quasicrystalline materials has reached a state of maturity such that basic structural characterisation tools, X-ray diffraction and electron diffraction, can be routinely applied in the studies of new or existing quasicrystalline materials. For the structural development of quasicrystalline materials, a quasi-unit cell model seems to explain all the details of true quasicrystalline phase formation and, thus, to satisfy the ambitions of researchers.

As for Al–Cu–Fe quasicrystals, their face-centered icosahedral atomic structure is composed of icosahedral atomic clusters containing close-packed planes and directions. A deep gap in the electron density of states is characteristic of the electronic structure of Al–Cu–Fe quasicrystals. These structural features of Al–Cu–Fe quasicrystals are linked to their special property combination: poor electrical and thermal conductivity, low surface energy and coefficient of friction as well as brittleness, work softening and high hardness. To enjoy the possibilities supplied by this new class of Al–Cu–Fe alloys, their production and the processing routes thereof to generate bulk materials and coatings are of primary importance. When prepared by conventional melting and casting, the quasicrystalline phase in Al–Cu–Fe system forms as a result of a peritectic reaction between β-AlFe, λ-Al_3Fe and the remaining liquid. However, crystalline phases often coexist with the stable quasicrystalline phase in the as-cast products. When completely quasicrystalline structure is required, additional annealing may be utilised, or the material may be synthesised by rapid solidification techniques, melt spinning and gas atomisation, or by mechanical alloying.

The trend is towards using quasicrystalline Al–Cu–Fe alloys increasingly as coating materials, where their good surface and physical properties find applications and poor mechanical properties are compensated by the substrate material. Quasicrystalline Al–Cu–Fe coatings can be best prepared by thermal spraying methods, and commercially available gas-atomised quasicrystalline powders make their utilisation easier. Another way to minimise the drawbacks of quasicrystalline Al–Cu–Fe alloys and make use of their advantages is to employ them as strengthening particles in composite materials. Significant growth in fundamental research concerning the interrelated effects of synthesis, processing, microstructure and properties of Al–Cu–Fe quasicrystals may provide new applications for quasicrystalline coatings and composite materials. Evidently, the greatest challenge for the future of Al–Cu–Fe quasicrystals is the production of industrial quantities of good quality quasicrystalline powders and coatings as well as of bulk materials thereof, to reach the expectations of the 20-year-old quasicrystal optimism.

Acknowledgements

The financial support by the Academy of Finland is gratefully acknowledged. The author is also thankful to Erja Turunen at VTT Technical Research Centre of Finland, Surface Engineering and Laser Processing, for fruitful discussions.

References

[1] D. Shechtman, I. Blech, D. Gratias, J.W. Cahn, Phys. Rev. Lett. 53 (1984) 1951–1953.
[2] C.J. Jenks, P.A. Thiel, J. Mol. Catal. A131 (1998) 301–306.
[3] Z.F. Li, B.X. Liu, Nucl. Instrum. Meth. Phys. Res. B 178 (2001) 224–228.
[4] J.R. Filho, R.R.L. de Carvalho, G.A. Farias, V.N. Freire, E.L. Albuquerque, Phys. B 305 (2001) 38–47.
[5] B.B. Bokhonov, E.Y. Ivanov, B.P. Tolochko, M.P. Sharaphutdinov, Mater. Sci. Eng. A278 (2000) 236–241.
[6] S. Yi, E.S. Park, J.B. Ok, W.T. Kim, D.H. Kim, Mater. Sci. Eng. A300 (2001) 312–315.
[7] B. Rubinstein, S.I. Ben-Abraham, Mater. Sci. Eng. A294–296 (2000) 418–420.
[8] F. Krumeich, C. Reich, M. Conrad, B. Harbrecht, Mater. Sci. Eng. A294–296 (2000) 152–155.
[9] M. Uchida, S. Horiuchi, Micron 31 (2000) 493–497.
[10] M. Conrad, F. Krumeich, C. Reich, B. Harbrecht, Mater. Sci. Eng. A294–296 (2000) 37–40.
[11] M.A. Shaz, R.K. Mandal, O.N. Srivastava, Mater. Sci. Eng. A304–306 (2001) 860–862.
[12] J.H. Lee, K.B. Kim, J.S. Lee, D.H. Kim, W.T. Kim, Mater. Sci. Eng. A304–306 (2001) 849–854.
[13] I.R. Fisher, M.J. Kramer, A.I. Goldman, Micron 31 (2000) 469–473.
[14] S. Kashimoto, H. Nakano, Y. Arichika, T. Ishimasa, S. Matsuo, Mater. Sci. Eng. A294–296 (2000) 588–591.
[15] T.J. Sato, E. Abe, A.P. Tsai, Mater. Sci. Eng. A304–306 (2001) 867–870.
[16] C. Li, J. Saida, A. Inoue, Scripta Mater. 42 (2000) 1077–1081.
[17] B.S. Murty, K. Hono, Mater. Sci. Eng. A312 (2001) 253–261.
[18] C. Fan, A. Inoue, Scripta Mater. 45 (2001) 115–120.
[19] P.D. Bloom, K.G. Baikerikar, J.U. Otaigbe, V.V. Sheares, Mater. Sci. Eng. 294–296 (2000) 156–159.
[20] M.F. Besser, T. Eisenhammer, Mater. Res. Soc. Bull. 10 (1997) 59–63.
[21] W.D. Callister, Materials Science and Engineering: An Introduction, Wiley, New York, 2000 871 pp.
[22] C. Giacovazzo, H.L. Monaco, D. Viterbo, F. Scordari, G. Gilli, G. Zanotti, M. Catti, Fundamentals of Crystallography, University Press, Oxford, 1992 654 pp.
[23] D. Shechtman, C.I. Lang, Mater. Res. Soc. Bull. 11 (1997) 40–42.
[24] D.J. Sordelet, J.M. Dubois, Mater. Res. Soc. Bull. 11 (1997) 34–37.
[25] J. Hafner, Curr. Opin. Solid State Mater. Sci. 4 (1999) 289–294.
[26] R. Penrose, Bull. Inst. Math. Applications 10 (1978) 266–271.

[27] A. Sinha, P. Ramachandrarao, Prog. Crystal Growth Characterisation 34 (1997) 147–156.
[28] P. Gummelt, C. Bandt, Mater. Sci. Eng. A294–296 (2000) 250–253.
[29] R. Lück, Mater. Sci. Eng. A294–296 (2000) 263–267.
[30] P. Bellingeri, P.M. Ossi, J. Alloys Comp. 316 (2001) 39–45.
[31] F. Gähler, Mater. Sci. Eng. A294–296 (2000) 199–204.
[32] E. Cockayne, Mater. Sci. Eng. A294–296 (2000) 224–227.
[33] C. Janot, J. Patera, Phys. Lett. A 233 (1997) 110–114.
[34] M. Feuerbacher, C. Metzmacher, M. Wollgarten, K. Urban, B. Baufeld, M. Bartsch, U. Messerschmidt, Mater. Sci. Eng. A233 (1997) 103–110.
[35] P.A. Bancel, P.A. Heiney, P.W. Stephens, A.I. Goldman, P.M. Horn, Phys. Rev. Lett. 54 (1985) 2422–2425.
[36] M. Duneau, Mater. Sci. Eng. A294–296 (2000) 192–198.
[37] P.J. Steinhardt, Mater. Sci. Eng. A294–296 (2000) 205–210.
[38] T. Egami, S.J. Poon, Mater. Sci. Eng. A99 (1988) 323–329.
[39] C. Janot, L. Loreto, R. Farinato, Mater. Sci. Eng. A294–296 (2000) 405–408.
[40] C.J. Jenks, P.A. Thiel, Mater. Res. Soc. Bull. 10 (1997) 55–58.
[41] V.E. Dmitrienko, S.B. Astaf'ev, M. Kléman, Mater. Sci. Eng. A294–296 (2000) 413–417.
[42] D. Joseph, V. Elser, Mater. Sci. Eng. A294–296 (2000) 254–257.
[43] K. Chattopadhyay, N. Ravishankar, R. Goswami, Prog. Crystal Growth Characterisation 34 (1997) 237–249.
[44] U. Mizutani, T. Takeuchi, V. Fournée, H. Sato, E. Banno, T. Ogoni, Scripta Mater. 44 (2001) 1181–1185.
[45] R. Chidambaram, M.K. Sanyal, P.M.G. Nambissan, P. Sen, Prog. Crystal Growth Characterisation 34 (1997) 207–220.
[46] A. Singh, S. Ranganathan, Prog. Mater. Sci. 42 (1997) 393–407.
[47] T. Fujiwara, Curr. Opin. Solid State Mater. Sci. 4 (1999) 295–301.
[48] Z.M. Stadnik, Mater. Sci. Eng. A294–296 (2000) 470–474.
[49] M.E. McHenry, R.C. O'Handley, Mater. Sci. Eng. A99 (1988) 377–383.
[50] J.B. Qiang, D.H. Wang, C.M. Bao, Y.M. Wang, W.P. Xu, M.L. Song, C. Dong, J. Mater. Res. 16 (2001) 2653–2660.
[51] A.P. Tsai, Mater. Res. Soc. Bull. 11 (1997) 43–47.
[52] A. Sadoc, Phil. Mag. Lett. 60 (1989) 195–200.
[53] F. Müller, M. Rosenberg, W. Liu, U. Köster, Mater. Sci. Eng. A134 (1991) 900–903.
[54] R.A. Brand, G. Coddens, A.I. Chumakov, A.J. Dianoux, Y. Calvayrac, Mater. Sci. Eng. A294–296 (2000) 662–665.
[55] R.A. Brand, J. Voss, Y. Calvayrac, J. Non-Crystall. Solids 287 (2001) 210–215.
[56] E. Belin-Ferré, J.M. Dubois, V. Fournée, P. Brunet, D.J. Sordelet, L.M. Zhang, Mater. Sci. Eng. A294–296 (2000) 821–828.
[57] G. Trambly de Laissardière, S. Roche, D. Mayou, Mater. Sci. Eng. A226–228 (1997) 986–989.
[58] C. Madel, G. Schwalbe, R. Haberkern, P. Häussler, Mater. Sci. Eng. A294–296 (2000) 535–538.
[59] J.H. Lee, K.B. Kim, J.S. Lee, D.H. Kim, W.T. Kim, Mater. Sci. Eng. A304–306 (2001) 849–854.
[60] A.P. Tsai, A. Inoue, T. Masumoto, Jpn. J. Appl. Phys. 26 (1987) L1505–L1507.
[61] A. Mele, H. Liu, R.E. Russo, X. Mao, A. Giardini, M. Satta, Appl. Surf. Sci. 186 (2002) 322–328.
[62] S.R. Nishitani, K.N. Ishihara, K.F. Kobayashi, P.H. Shingu, Mater. Sci. Eng. A99 (1988) 443–447.
[63] R. Nicula, A. Jianu, C. Grigoriu, T. Barfels, E. Burkel, Mater. Sci. Eng. A294–296 (2000) 86–89.
[64] M. Takeda, S. Sakai, A. Kawasaki, Y. Hattori, M. Katoh, Mater. Sci. Eng. A294–296 (2000) 842–845.
[65] R. Teghil, L. D'Alessio, M.A. Simone, M. Zaccagnino, D. Ferro, D.J. Sordelet, Appl. Surf. Sci. 168 (2000) 267–269.
[66] A. Kanjilal, R. Singh, R. Chatterjee, Mater. Res. Bull. 36 (2001) 2323–2331.
[67] T. Grenet, F. Giroud, C. Loubet, J.L. Joulaud, M. Capitan, Mater. Sci. Eng. A294–296 (2000) 838–841.
[68] Y. Ding, D.O. Northwood, A.T. Atpas, Surf. Coatings Tech. 96 (1997) 140–147.
[69] V. Srinivas, R.A. Dunlap, Mater. Res. Bull. 30 (1995) 581–583.
[70] J.M. Dubois, Mater. Sci. Eng. A294–296 (2000) 4–9.
[71] P. Brunet, L.M. Zhang, D.J. Sordelet, M. Besser, J.M. Dubois, Mater. Sci. Eng. A294–296 (2000) 74–78.
[72] A.P. Tsai, T.J. Sato, J.Q. Guo, T. Hirano, J. Non-Crystall. Solids 250–252 (1999) 833–838.
[73] I.R. Fisher, M.J. Kramer, Z. Islam, T.A. Wiener, A. Kracher, A.R. Ross, T.A. Lograsso, A.I. Goldman, P.C. Canfield, Mater. Sci. Eng. A294–296 (2000) 10–16.
[74] S. Yi, K.B. Kim, E. Fleury, W.T. Kim, D.H. Kim, Mater. Lett. 52 (2002) 75–79.
[75] S. Wojciechowski, J. Mater. Proc. Tech. 106 (2000) 230–235.
[76] V. Venkateswara Rao, T.R. Anantharaman, Mater. Sci. Eng. A99 (1988) 393–398.
[77] Y. Sakurai, C. Kokubu, Y. Tanaka, Y. Watanabe, M. Masuda, S. Nanao, Mater. Sci. Eng. A99 (1988) 423–426.
[78] T. Takeuchi, T. Mizuno, E. Banno, U. Mizutani, Mater. Sci. Eng. A294–296 (2000) 522–526.
[79] V.I. Tkach, A.I. Limanovskii, S.N. Denisenko, S.G. Rassolov, Mater. Sci. Eng. A323 (2002) 91–96.
[80] E.S. Humphreys, P.J. Warren, A. Cerezo, Mater. Sci. Eng. A250 (1998) 158–163.
[81] E. Klar, J.W. Fesko, Metals Handbook, Powder Metallurgy, ASM, Ohio, 1984, 897 pp.
[82] Y. Ji, M. Kallio, T. Tiainen, Scripta Mater. 42 (2000) 1017–1023.
[83] C. Suryanarayana, E. Ivanov, V.V. Boldyrev, Mater. Sci. Eng. A304–306 (2001) 151–158.
[84] F. Schurack, J. Eckert, L. Schultz, Mater. Sci. Eng. A294–296 (2000) 164–167.
[85] S. Yi, K.B. Kim, W.T. Kim, D.H. Kim, Scripta Mater. 44 (2001) 1757–1760.
[86] N. Asahi, Mater. Sci. Eng. A226–228 (1997) 67–69.
[87] J. Eckert, L. Schultz, K. Urban, Mater. Sci. Eng. A133 (1991) 393–397.
[88] C. Suryanarayana, Prog. Mater. Sci. 46 (2001) 1–184.
[89] J.M. Cairney, P.R. Munroe, D.J. Sordelet, J. Microsc. 201 (2001) 201–211.
[90] F. Schurack, J. Eckert, L. Schultz, Acta Mater. 49 (2001) 1351–1361.
[91] F. Schurack, J. Eckert, L. Schultz, Nanostructured Mater. 12 (1999) 107–110.
[92] A.J. Bradley, H.J. Goldschmidt, J. Inst. Met. 65 (1939) 403–418.
[93] F. Faudot, A. Quivy, Y. Calvayrac, D. Gratias, M. Harmelin, Mater. Sci. Eng. A133 (1991) 383–387.
[94] J. Gui, J. Wang, R. Wang, D. Wang, J. Liu, F. Chen, J. Mater. Res. 16 (2001) 1037–1046.
[95] Y. Yokoyama, K. Fukaura, H. Sunada, R. Note, K. Hiraga, A. Inoue, Mater. Sci. Eng. A294–296 (2000) 68–73.
[96] Y. Yokoyama, R. Note, K. Fukaura, H. Sanada, K. Hiraga, A. Inoue, Mater. Trans. Jpn. Inst. Met. 41 (2000) 1583–1588.
[97] R. Van Buuren, J. Sietsma, A. van den Beukel, Mater. Sci. Eng. A134 (1991) 951–954.
[98] S.M. Lee, B.H. Kim, D.H. Kim, W.T. Kim, J. Mater. Res. 16 (2001) 1535–1540.
[99] A. Waseda, K. Kimura, H. Ino, Mater. Trans. Jpn. Inst. Met. 34 (1993) 169–177.
[100] A. Waseda, K. Kimura, H. Ino, Mater. Sci. Eng. A181–182 (1994) 762–765.
[101] G. Rosas, R. Perez, Mater. Sci. Eng. A298 (2001) 79–83.
[102] G. Rosas, R. Perez, Mater. Lett. 36 (1998) 229–234.
[103] G. Rosas, R. Perez, Mater. Lett. 47 (2001) 225–230.
[104] D. Holland-Moritz, J. Schroers, B. Grushko, D.M. Herlach, K. Urban, Mater. Sci. Eng. A226–228 (1997) 976–980.

[105] D. Holland-Moritz, J. Schroers, D.M. Herlach, B. Grushko, K. Urban, Acta Mater. 46 (1998) 1601–1615.
[106] F.X. Zhang, W.K. Wang, Mater. Sci. Eng. A205 (1996) 214–220.
[107] S.M. Lee, H.J. Jeon, B.H. Kim, W.T. Kim, D.H. Kim, Mater. Sci. Eng. A304–306 (2001) 871–878.
[108] A.P. Tsai, A. Inoue, T. Masumoto, J. Mater. Sci. Lett. 6 (1987) 1403–1405.
[109] R.A. Brand, J. Voss, Y. Calvayrac, Mater. Sci. Eng. A294–296 (2000) 666–669.
[110] R. Divakar, D. Sundararaman, V.S. Raghunathan, Prog. Crystal Growth Characterisation 34 (1997) 263–269.
[111] K. Edagawa, A. Waseda, K. Kimura, H. Ino, Mater. Sci. Eng. A134 (1991) 939–942.
[112] A. Waseda, K. Edagawa, H. Ino, Phil. Mag. Lett. 62 (1990) 183–186.
[113] S. De Palo, S. Usmani, S. Sampath, D.J. Sordelet, M. Besser, Friction and Wear Behaviour of Thermally Sprayed Al–Cu–Fe Quasicrystal Coatings. A United Forum For Scientific and Technological Advances, ASM International, Ohio, 1997.
[114] M. Jono, Y. Matsuo, Y. Ishii, Mater. Sci. Eng. A294–296 (2000) 680–684.
[115] W. Liu, U. Köster, Mater. Sci. Eng. A133 (1991) 388–392.
[116] M. Boudard, A. Létoublon, M. de Boissieu, T. Ishimasa, M. Mori, E. Elkaim, J.P. Lauriat, Mater. Sci. Eng. A294–296 (2000) 217–220.
[117] L. Wang, Z.C. Tan, J.B. Zhang, S.H. Meng, L.M. Zhang, Q.G. Zhou, C. Dong, Thermochim. Acta 331 (1999) 21–25.
[118] W.A. Cassada, G.J. Shiflet, S.J. Poon, J. Microsc. 146 (1987) 323–335.
[119] S.M. Lee, J.H. Jung, E. Fleury, W.T. Kim, D.H. Kim, Mater. Sci. Eng. A294–296 (2000) 99–103.
[120] V. Srinivas, P. Barua, B.S. Murty, Mater. Sci. Eng. A294–296 (2000) 65–67.
[121] P. Barua, B.S. Murty, V. Srinivas, Mater. Sci. Eng. A304–306 (2001) 863–866.
[122] N. Asahi, T. Maki, S. Matsumoto, T. Sawai, Mater. Sci. Eng. A181–182 (1994) 841–844.
[123] K.B. Kim, S.H. Kim, W.T. Kim, D.H. Kim, K.T. Hong, Mater. Sci. Eng. A304–306 (2001) 822–829.
[124] A.I. Salimon, A.M. Korsunsky, E.V. Shelekhov, T.A. Sviridova, S.D. Kaloshkin, V.S. Tcherdyntsev, Y.V. Baldokhin, Acta Mater. 49 (2001) 1821–1833.
[125] M. Miglierini, S. Nasu, Mater. Trans. Jpn. Inst. Met. 34 (1993) 178–187.
[126] F. Audebert, R. Colaço, R. Vilar, H. Sirkin, Scripta Mater. 40 (1999) 551–557.
[127] E. Fleury, S.M. Lee, W.T. Kim, D.H. Kim, J. Non-Crystall. Solids 278 (2000) 194–204.
[128] D.J. Sordelet, M.F. Besser, I.E. Anderson, J. Thermal Spray Tech. 5 (1996) 161–174.
[129] D.J. Sordelet, M.J. Kramer, O. Unal, J. Thermal Spray Tech. 4 (1995) 235–244.
[130] K. Kimura, H. Yamane, T. Hashimoto, S. Takeuchi, Mater. Sci. Eng. A99 (1988) 435–438.
[131] Ö. Rapp, Mater. Sci. Eng. A294–296 (2000) 458–463.
[132] C. Berger, J. Delahaye, T. Grenet, T. Schaub, G. Fourcaudot, J.P. Brison, J.J. Préjean, Phys. B 280 (2000) 262–263.
[133] C. Janot, Europhysics News 27 (1996) 60–64.
[134] R. Tamura, A. Waseda, K. Kimura, H. Ino, Mater. Sci. Eng. A181–182 (1994) 794–797.
[135] A. Bilušic, D. Pavuna, A. Smontara, Vacuum 61 (2001) 345–348.
[136] L. Solymar, D. Walsh, Lectures on the Electrical Properties of Materials, University Press, Oxford, UK, 1993 482 pp.
[137] C.V. Landauro, H. Solbrig, Mater. Sci. Eng. A294–296 (2000) 600–603.
[138] T. Grenet, F. Giroud, Mater. Sci. Eng. A294–296 (2000) 576–579.
[139] E. Belin, Z. Dankhazi, Mater. Sci. Eng. A181–182 (1994) 717–721.
[140] T. Eisenhammer, A. Mahr, A. Haugeneder, W. Assmann, Solar Energy Mater. Solar Cells 46 (1997) 53–65.
[141] P. Archambault, C. Janot, Mater. Res. Soc. Bull. 10 (1997) 48–53.
[142] A. Bilušic, A. Smontara, J.C. Lasjaunias, J. Ivkov, Y. Calvayrac, Mater. Sci. Eng. A294–296 (2000) 711–714.
[143] A. Smontara, J.C. Lasjaunias, C. Paulsen, A. Bilušic, Y. Calvayrac, Mater. Sci. Eng. A294–296 (2000) 706–710.
[144] A.M. Korsunsky, A.I. Salimon, I. Pape, A.M. Polyakov, A.N. Fitch, Scripta Mater. 44 (2001) 217–222.
[145] T. Cai, F. Shi, Z. Shen, M. Gierer, A.I. Goldman, M.J. Kramer, C.J. Jenks, T.A. Lograsso, D.W. Delaney, P.A. Thiel, M.A. Van Hove, Surf. Sci. 495 (2001) 19–34.
[146] J.C. Park, W.T. Kim, D.H. Kim, J.R. Kim, Mater. Sci. Eng. A304–306 (2001) 225–230.
[147] L.M. Zhang, H.C. Zhang, Q.G. Zhou, C. Dong, Wear 225–229 (1999) 784–788.
[148] D. Popović, D. Naumović, M. Bovet, C. Koitzsch, L. Schlapbach, P. Aebi, Surf. Sci. 492 (2001) 294–304.
[149] B.I. Wehner, J. Meinhardt, U. Köster, H. Alves, N. Eliaz, D. Eliezer, Mater. Sci. Eng. A226–228 (1997) 1008–1011.
[150] B.I. Wehner, U. Köster, A. Rüdiger, C. Pieper, D.J. Sordelet, Mater. Sci. Eng. A294–296 (2000) 830–833.
[151] A. Rüdiger, U. Köster, Mater. Sci. Eng. A294–296 (2000) 890–893.
[152] A. Rüdiger, U. Köster, J. Non-Crystall. Solids 250–252 (1999) 898–902.
[153] A.P. Tsai, M. Yoshimura, Appl. Catal. A 214 (2001) 237–241.
[154] G.S. Song, K.B. Kim, E. Fleury, W.T. Kim, D.H. Kim, J. Mater. Sci. Lett. 20 (2001) 1293–1296.
[155] G.S. Song, S.H. Kim, W.T. Kim, D.H. Kim, J. Mater. Sci. Lett. 20 (2001) 1281–1284.
[156] K.F. Kelton, P.C. Gibbons, Mater. Res. Soc. Bull. 10 (1997) 69–72.
[157] D.J. Sordelet, M.F. Besser, J.L. Logsdon, Mater. Sci. Eng. A255 (1998) 54–65.
[158] J.S. Wu, V. Brien, P. Brunet, C. Dong, J.M. Dubois, Mater. Sci. Eng. 294–296 (2000) 846–849.
[159] K. Urban, M. Feuerbacher, M. Wollgarten, Mater. Res. Soc. Bull. 10 (1997) 65–68.
[160] K. Edagawa, Mater. Sci. Eng. A309–310 (2001) 528–538.
[161] M.A. Fradkin, Mater. Sci. Eng. A294–296 (2000) 795–798.
[162] R. Tamura, S. Takeuchi, K. Edagawa, Mater. Sci. Eng. A309–310 (2001) 552–556.
[163] S.S. Kang, J.M. Dubois, Phil. Mag. A 66 b (1992) 151–163.
[164] L. Bresson, D. Gratias, J. Non-Crystall. Solids 153–154 (1993) 468–472.
[165] U. Köster, H. Liebertz, W. Liu, Mater. Sci. Eng. A181–182 (1994) 777–780.
[166] T. Tei, K. Edagawa, S. Takeuchi, K. Masuda-Jindo, Mater. Sci. Eng. A134 (1991) 904–907.
[167] B. Wolf, K.O. Bambauer, P. Paufler, Mater. Sci. Eng. A298 (2001) 284–295.
[168] R. Wang, W. Yang, J. Gui, K. Urban, Mater. Sci. Eng. A294–296 (2000) 742–747.
[169] M. Feuerbacher, C. Metzmacher, M. Wollgarten, K. Urban, B. Baufeld, M. Bartsch, U. Messerschmidt, Mater. Sci. Eng. A226–228 (1997) 943–949.
[170] J.E. Shield, M.J. Kramer, J. Mater. Res. 12 (1997) 2043–2047.
[171] M.X. Dai, K. Urban, Phil. Mag. Lett. 67 (1993) 67–71.
[172] J.E. Shield, M.J. Kramer, Phil. Mag. Lett. 69 (1994) 115–121.
[173] Z. Zhang, M. Wollgarten, K. Urban, Phil. Mag. Lett. 61 (1990) 125–131.
[174] H.M. Kimura, K. Sasamori, A. Inoue, Mater. Sci. Eng. A294–296 (2000) 168–172.
[175] E. Giacometti, N. Baluc, J. Bonneville, Mater. Sci. Eng. A294–296 (2000) 777–780.

[176] E. Giacometti, P. Guyot, N. Baluc, J. Bonneville, Mater. Sci. Eng. A319–321 (2001) 429–433.
[177] E. Giacometti, N. Baluc, J. Bonneville, J. Rabier, Scripta Mater. 41 (1999) 989–994.
[178] S.N. Dub, Y.V. Milman, D.V. Lotsko, A.N. Belous, J. Mater. Sci. Lett. 20 (2001) 1043–1045.
[179] U. Ponkratz, R. Nicula, A. Jianu, E. Burkel, J. Non-Crystall. Solids 250–252 (1999) 844–848.
[180] F. Cyrot-Lackmann, Mater. Sci. Eng. A294–296 (2000) 611–612.
[181] D.J. Sordelet, S.D. Widener, Y. Tang, M.F. Besser, Mater. Sci. Eng. A294–296 (2000) 834–837.